Munich-Centre for Advanced Photonics

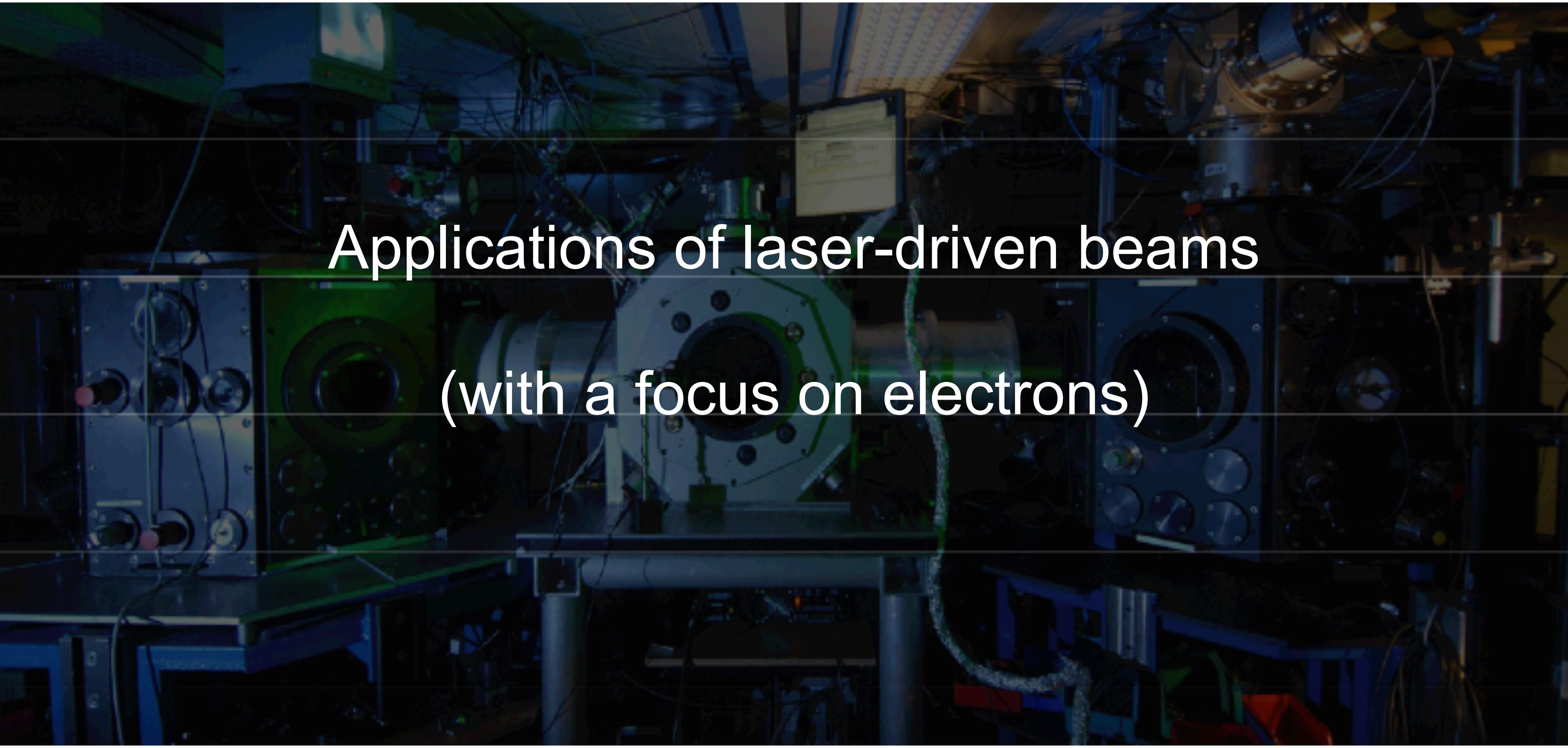

Applications of laser-driven beams

(with a focus on electrons)

Stefan Karsch
Ludwig-Maximilians-Universität München/
MPI für Quantenoptik
Garching, Germany

Motivation: X-ray tumour diagnosis

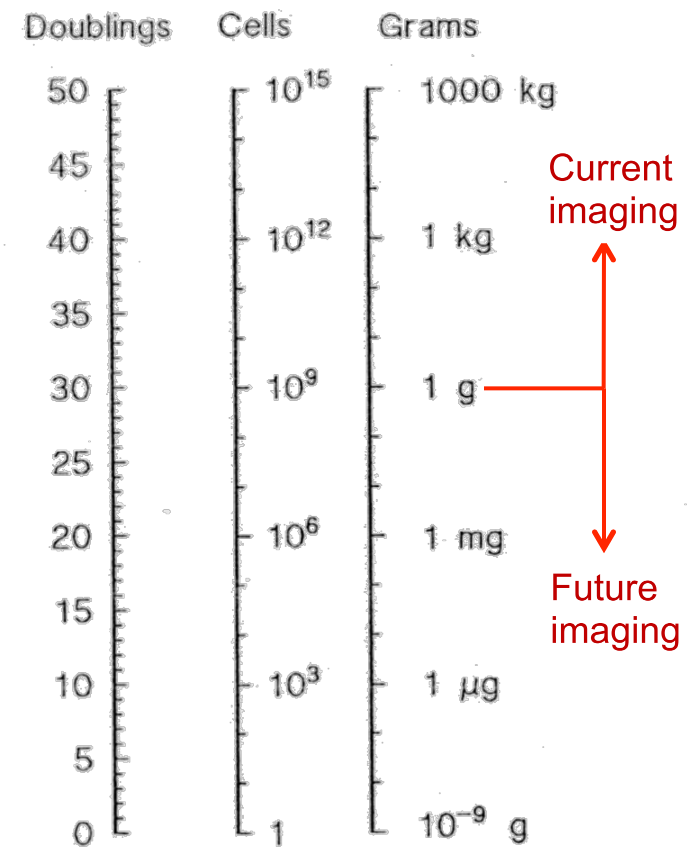

Gordon Steel, Basic Clinical Radiobiology, 2002

Clinical evidence:

Primary tumours of up to approx. 10^6 cells have generally not metastasized. Local tumor therapy might be successful.

Strategy

- Early tumour diagnosis (while diameter is below 1 mm)
- Local non-invasive radiation therapy using various beam types and treatment techniques.

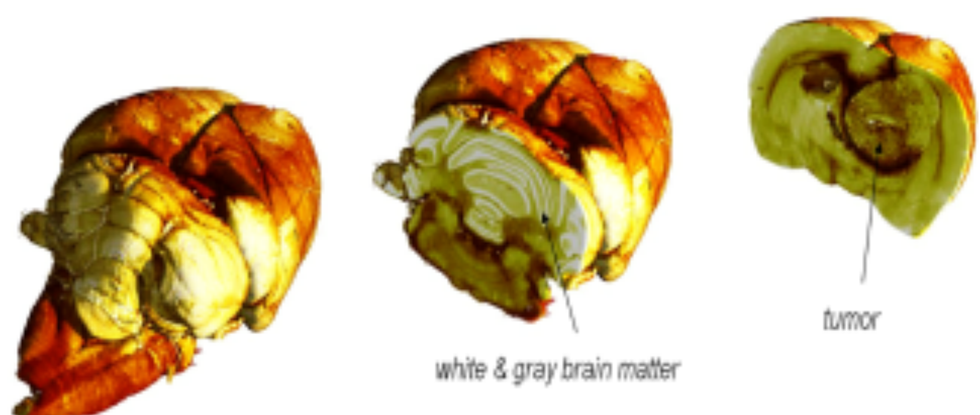

F. Pfeiffer et al., PMB 52, 6923 (2007).

Phase-contrast tomography of a rat brain

Phase-contrast CT allows excellent soft-tissue discrimination

conventional CT

phase contrast CT

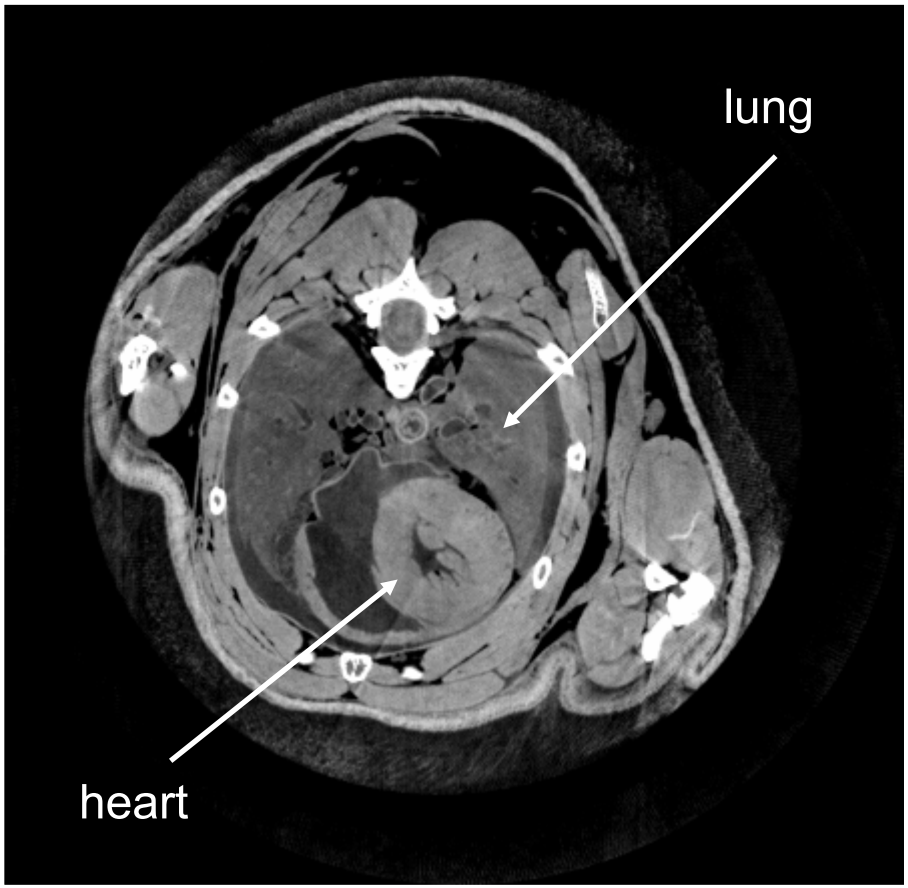

Slices through a mouse thorax using equal radiation dose.

(F. Pfeiffer)

Phase Contrast Imaging

Requirements:
sufficient degree of spatial coherence
a high resolution detector

Modulation of the phase much stronger than absorption

Refractive index: $n = 1-\delta-i\beta$

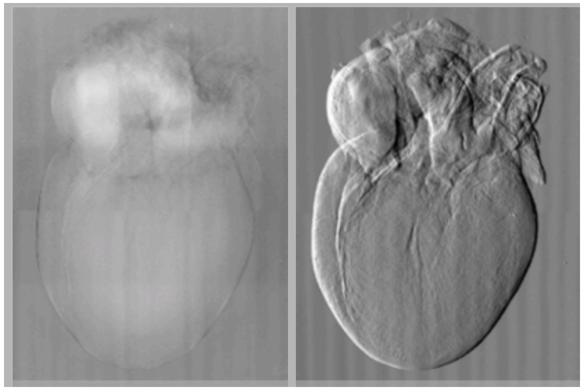

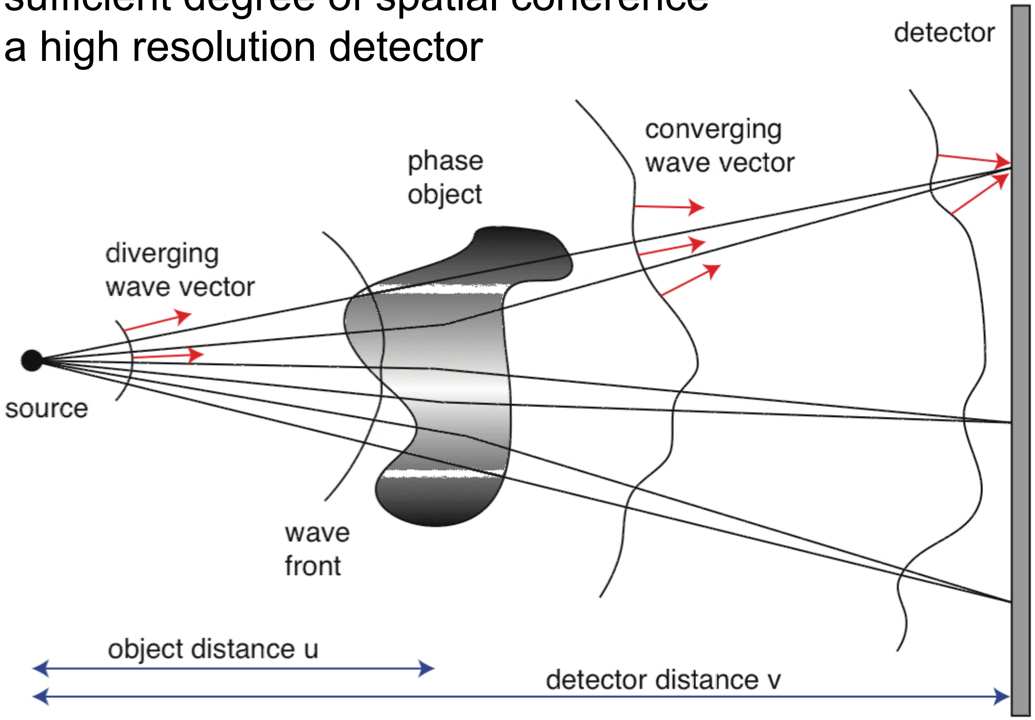

$$\text{Brilliance} = \frac{\text{photons}}{\boxed{\text{mm}^2 \cdot \text{mrad}^2} \cdot \boxed{\text{s} \cdot 0.1\%\ \text{bandwidth}}}$$

transv. emittance (=phase space area)

long. emittance

High photon flux

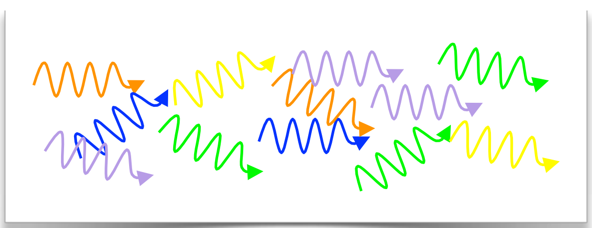

Low divergence

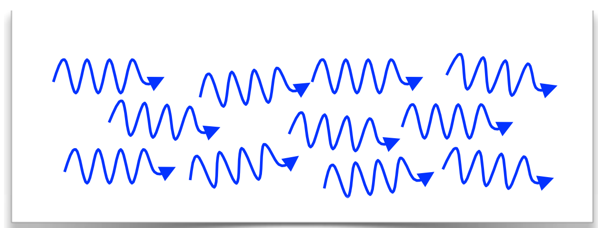

Small band-width

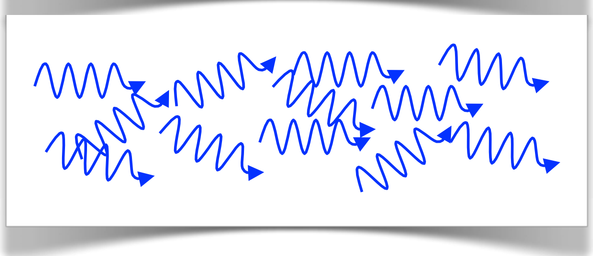

Small source size

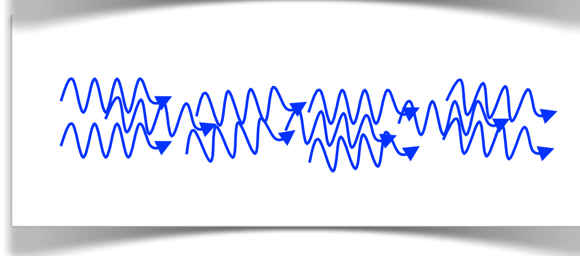

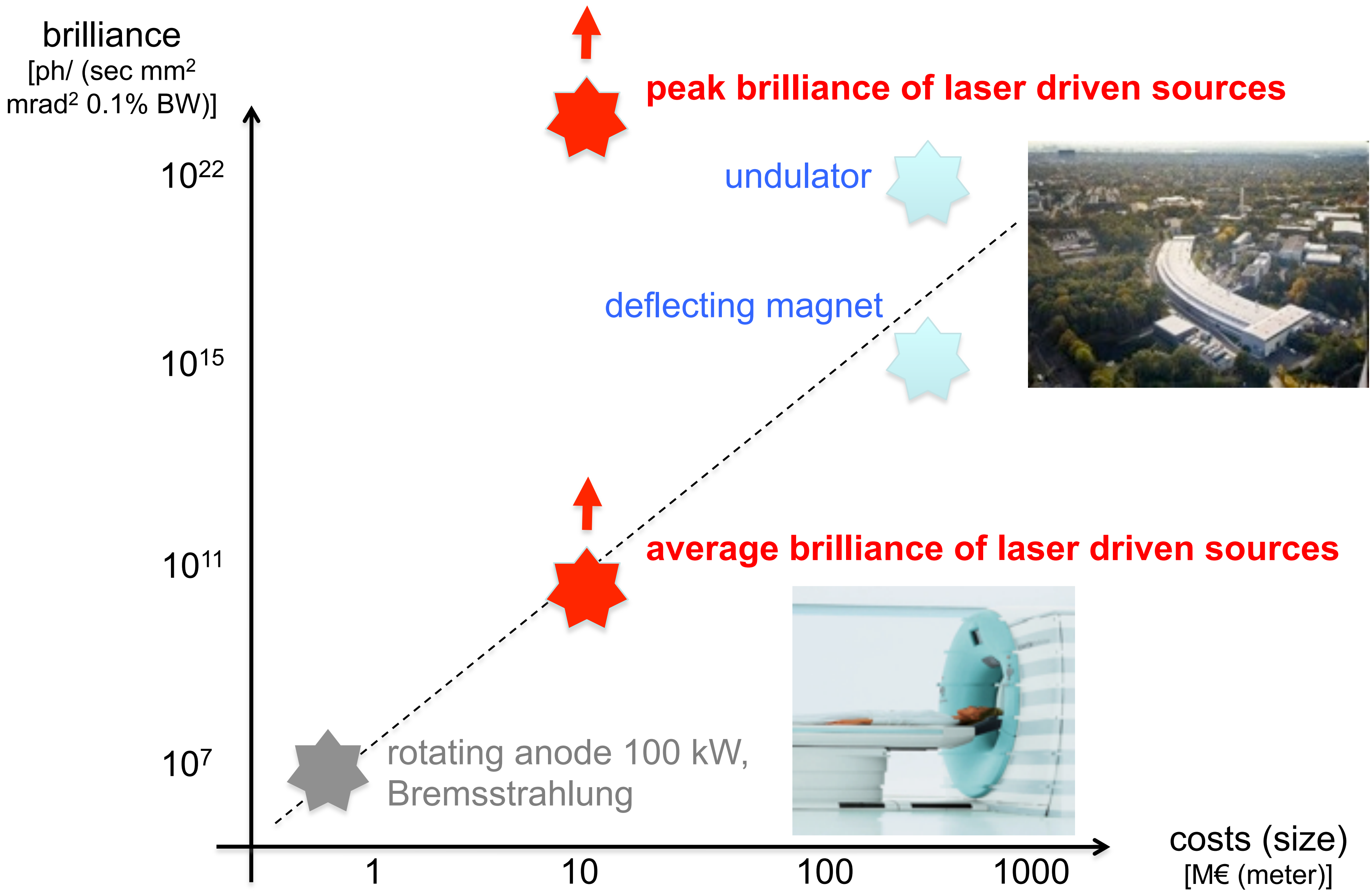
brilliance
[ph/ (sec mm²
mrad² 0.1% BW)]
10^{22}
10^{15}
10^{11}
10^{7}
peak brilliance of laser driven sources
undulator
deflecting magnet
average brilliance of laser driven sources
rotating anode 100 kW,
Bremsstrahlung
1
10
100
1000
costs (size)
[M€ (meter)]

„Wiggly“ electron X-ray sources: Ingredients: relativistic electron beam +

undulator

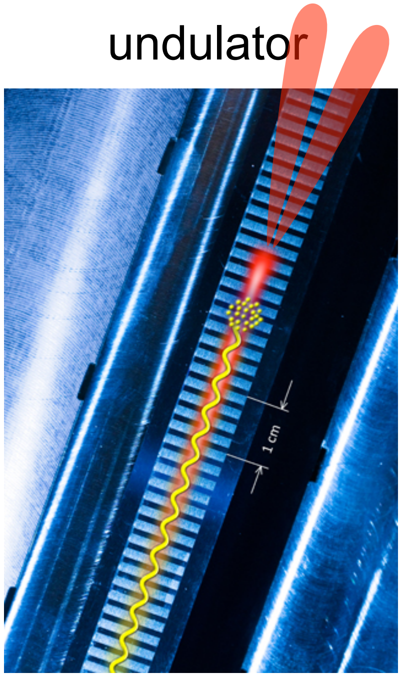

undulator radiation, FEL
100‘s eV - keV
$\lambda_u \approx 1$cm

$$\lambda_{x-ray} = \frac{\lambda_u}{2\gamma^2}\left(1 + \frac{K^2}{2} + \gamma^2\theta^2\right)$$

plasma fields

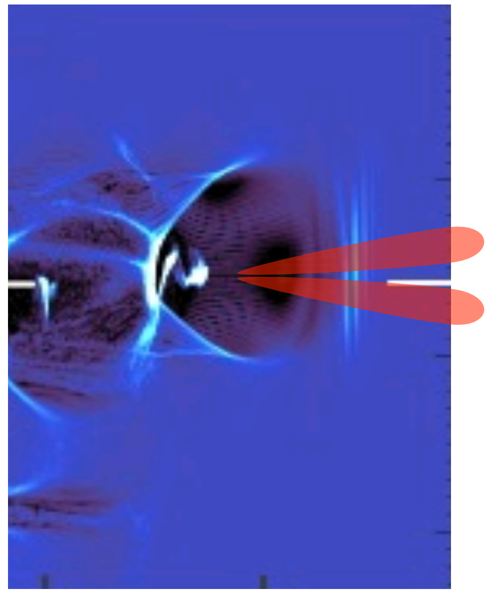

Betatron radiation
keV – 10‘s keV
$\lambda_b \approx 500$µm

laser fields

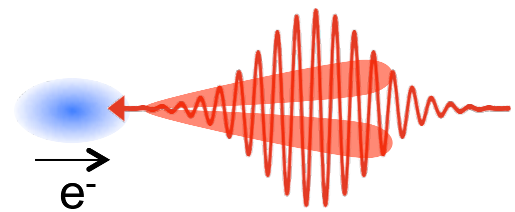

Thomson scattering
10‘s keV - MeV
$\lambda_l \approx 1$µm

$$\lambda_{x-ray} = \frac{\lambda_l}{4\gamma^2}\left(1 + \frac{a_0^2}{2} + \gamma^2\theta^2\right)$$

Ingredient No.1:

Electron beams

A. Popp, M. Heigoldt, S.W. Chou et al.

Source: Kent Nishimura/Getty Images North America (2009)

Plasma acceleration: prediction and reality

VOLUME 43, NUMBER 4 PHYSICAL REVIEW LETTERS 23 JULY 1979

Laser Electron Accelerator

T. Tajima and J. M. Dawson
Department of Physics, University of California, Los Angeles, California 90024
(Received 9 March 1979)

An intense electromagnetic pulse can create a weak of plasma oscillations through the action of the nonlinear ponderomotive force. Electrons trapped in the wake can be accelerated to high energy. Existing glass lasers of power density 10^{18}W/cm^2 shone on plasmas of densities 10^{18} cm^{-3} can yield gigaelectronvolts of electron energy per centimeter of acceleration distance. This acceleration mechanism is demonstrated through computer simulation. Applications to accelerators and pulsers are examined.

2006:

40 TW laser pulse

1 GeV, 30 pC
3×10^{18} W/cm^2
$n_e=4.3\times10^{18}$ cm^{-3}
$L_{acc.} \approx 1$ cm

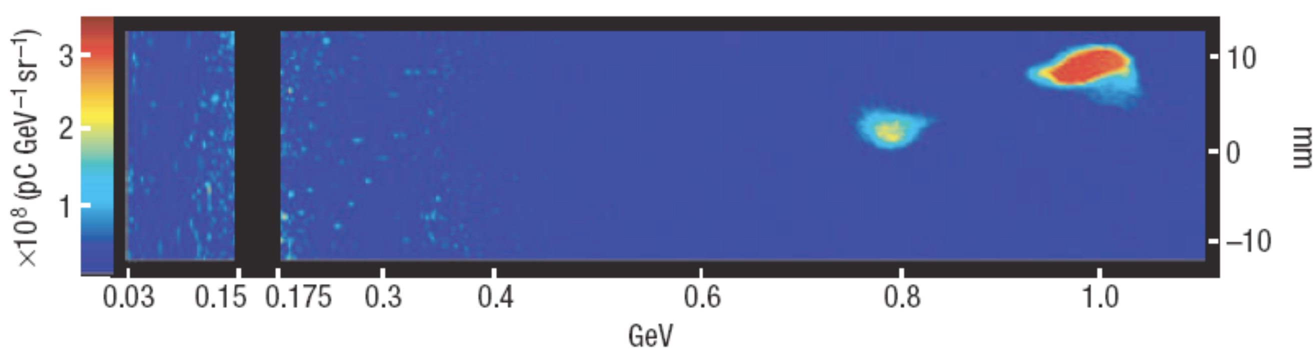

W.P. Leemans et al, Nature Physics 2, 696, 2006

Stable beams by using stagnant flow gas cell

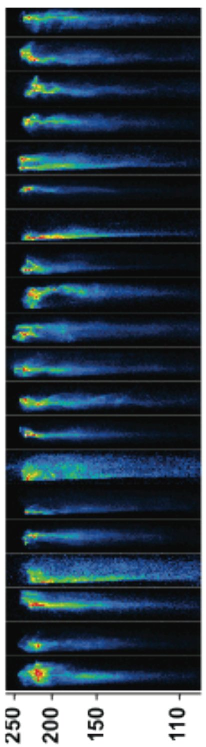

energy (MeV)

ATLAS 25
0.85 J on target
37 fs
Capillary
peak energy ~ 200 MeV
total charge ~ 30 pC

ATLAS 60
1.5 J on target
25 fs
Gas cell
peak energy ~ 500 MeV
total charge ~ 100 pC

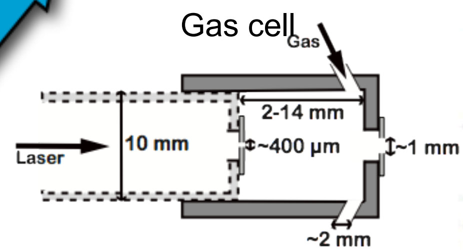

a0=1.86
≈1 J on target

a0=2.28
1.5 J on target

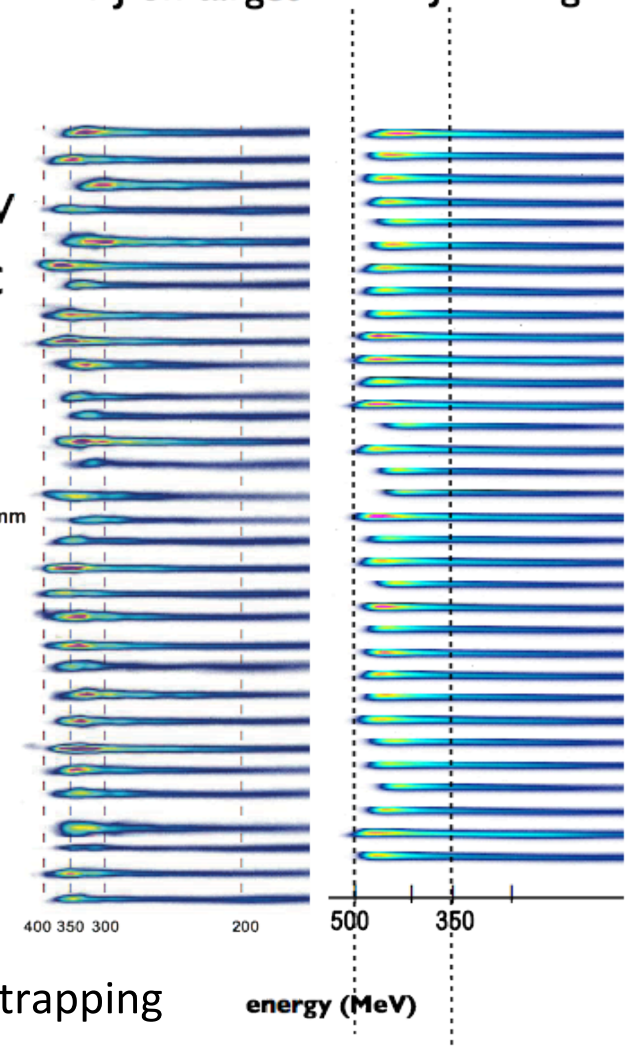

energy (MeV)

→ Blowout regime, continuous trapping

Osterhoff, SK et al., PRL 101, 085002 (2008)

Munich-Centre for Advanced Photonics

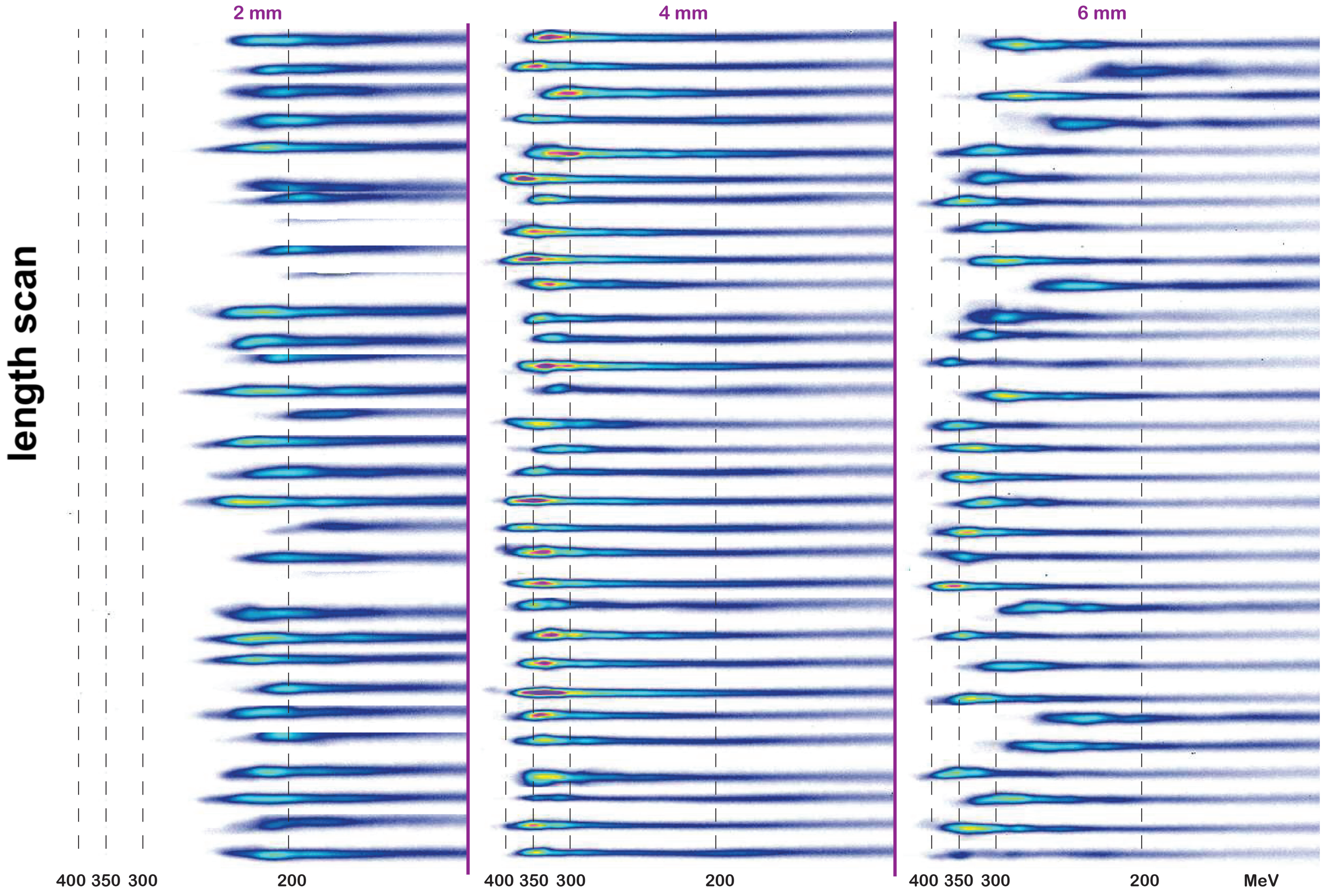

cut-off energy

130 mbar = 6.4 x 10^{18} cm^{-3}

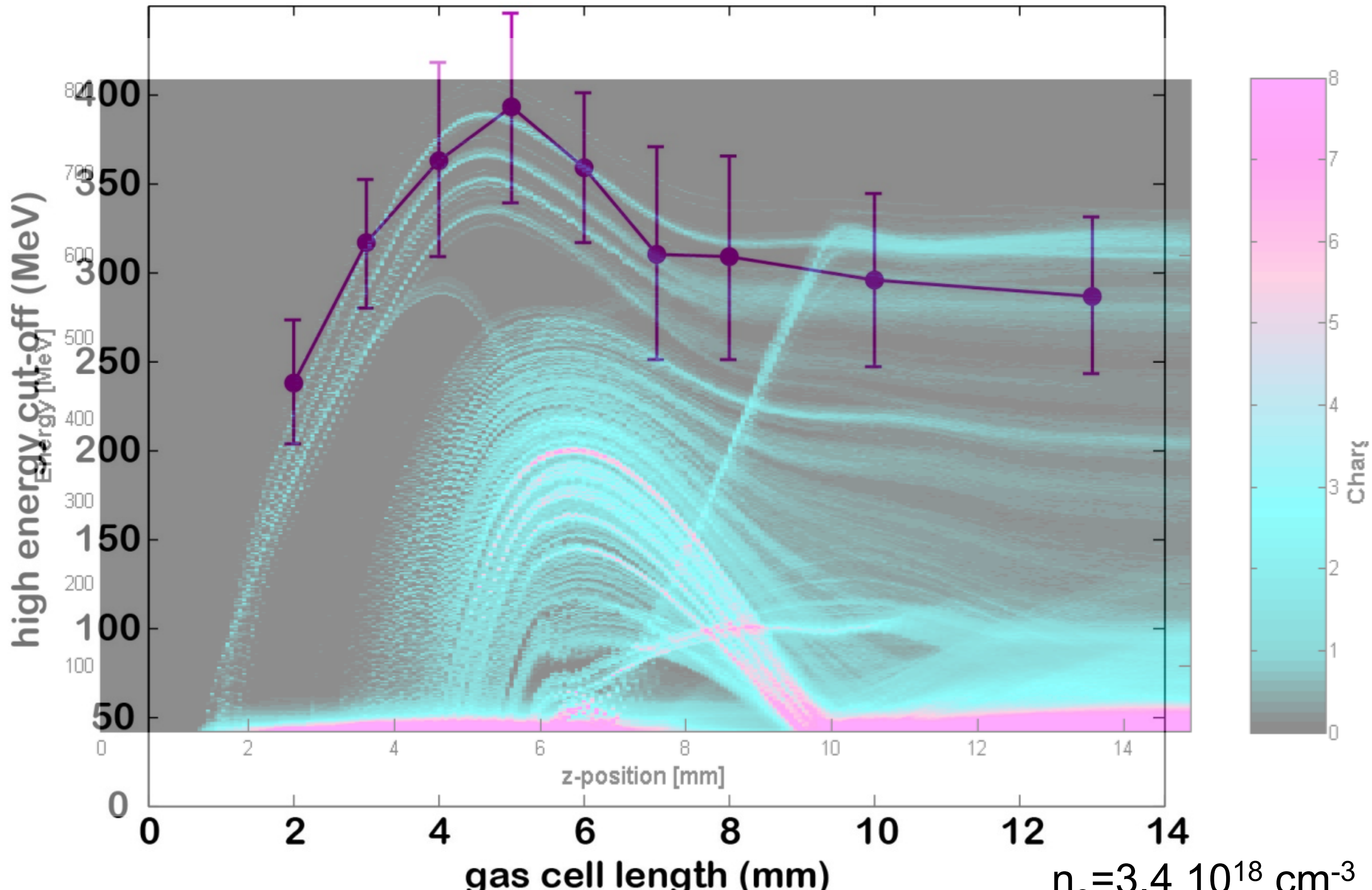

n_e=3.4 10^{18} cm^{-3}

A. Popp et al., in preparation

3d PIC simulation (OSIRIS) by J. Vieira

High-charge 0.5 GeV beams from a 1.5J, 60 TW laser
Halo at highest energy hints at 4:1 betatron-laser resonance and resonant excitation

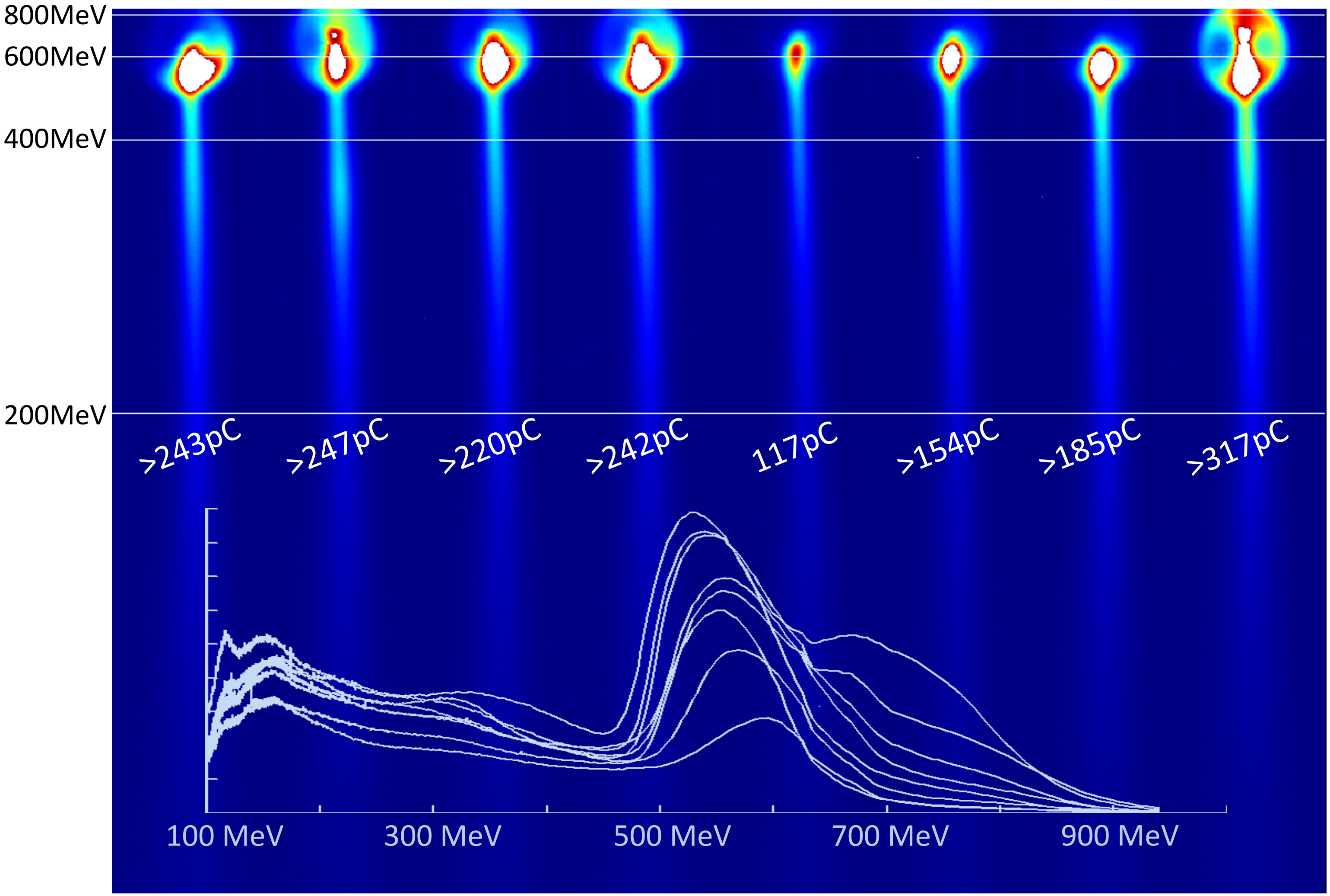

Emittance measurement by direct imaging of electron beam inside the source:

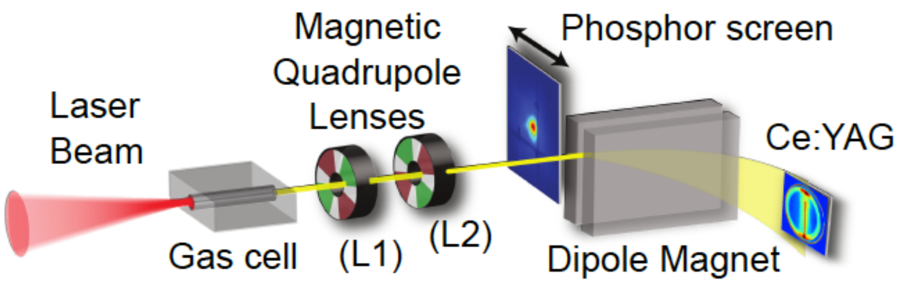

RMS beam size in Ce:YAG crstal after 30 x magnification by the lenses

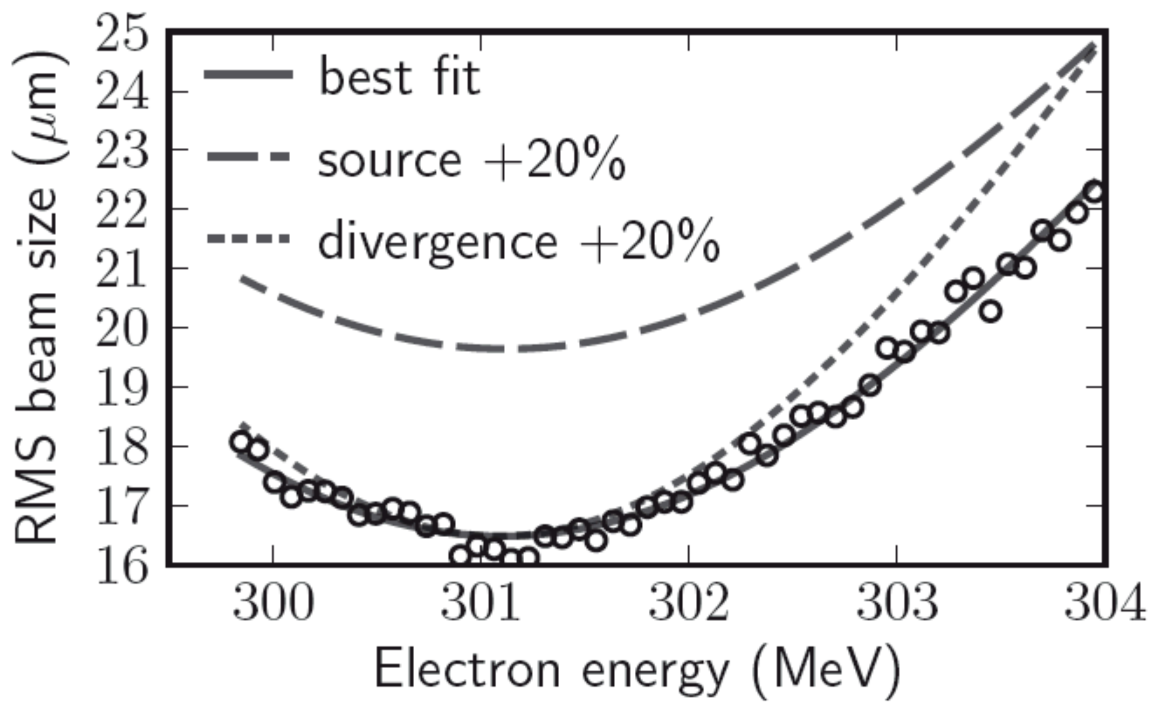

Normalized emittance: 0.14 π mm mrad

Temporal characterization by coherent TR spectroscopy

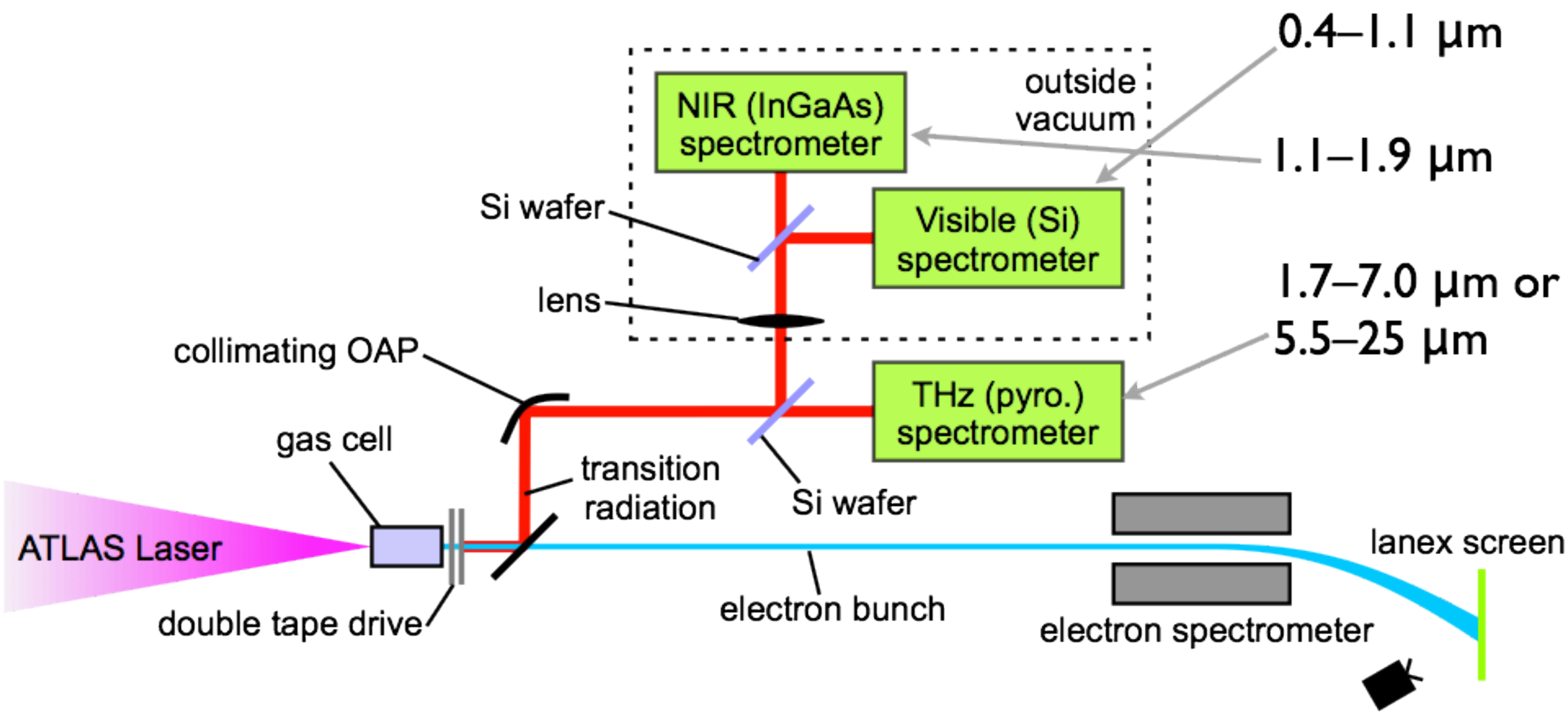

pressure 70 mbar, density 3.7×10^{18} cm^{-3}

8 mm gas cell,
smooth spectrum
5.1 fs FWHM

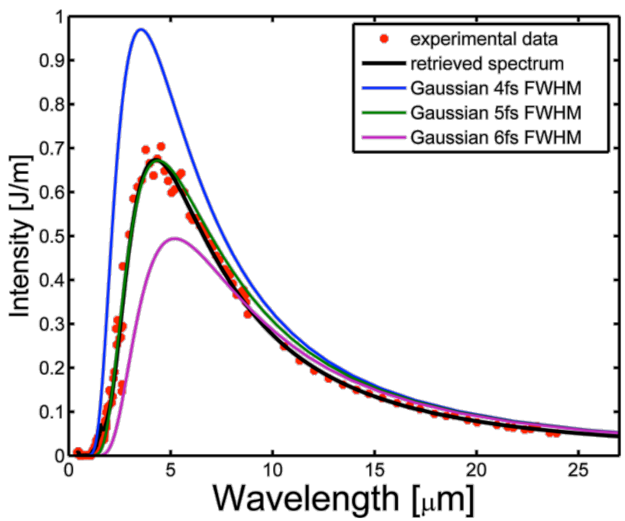

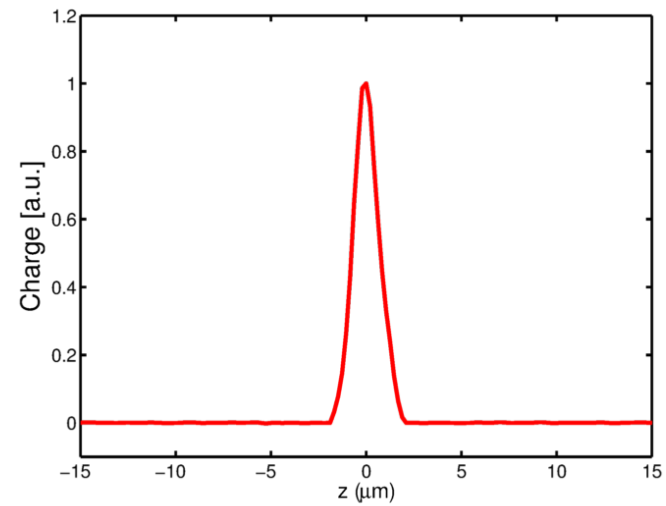

12 mm gas cell,
modulated spectrum
3.9 fs FWHM

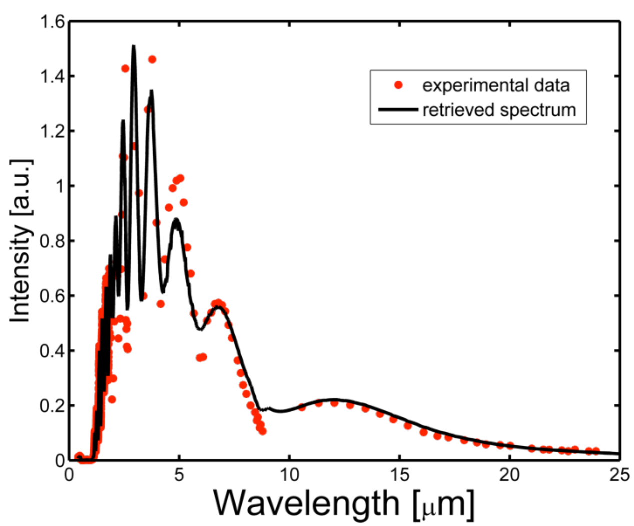

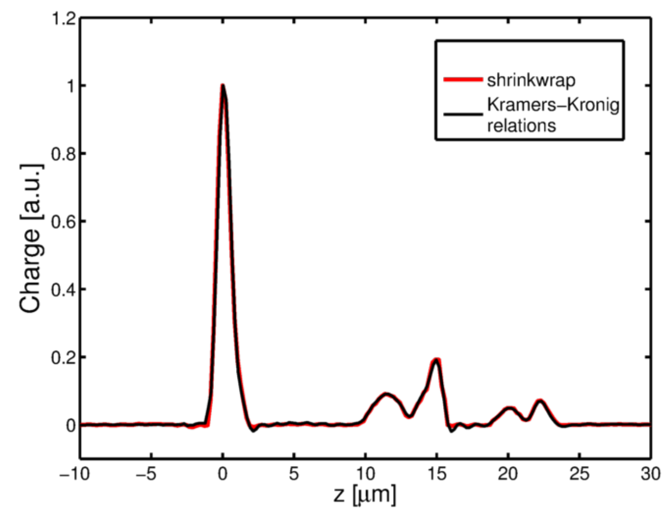

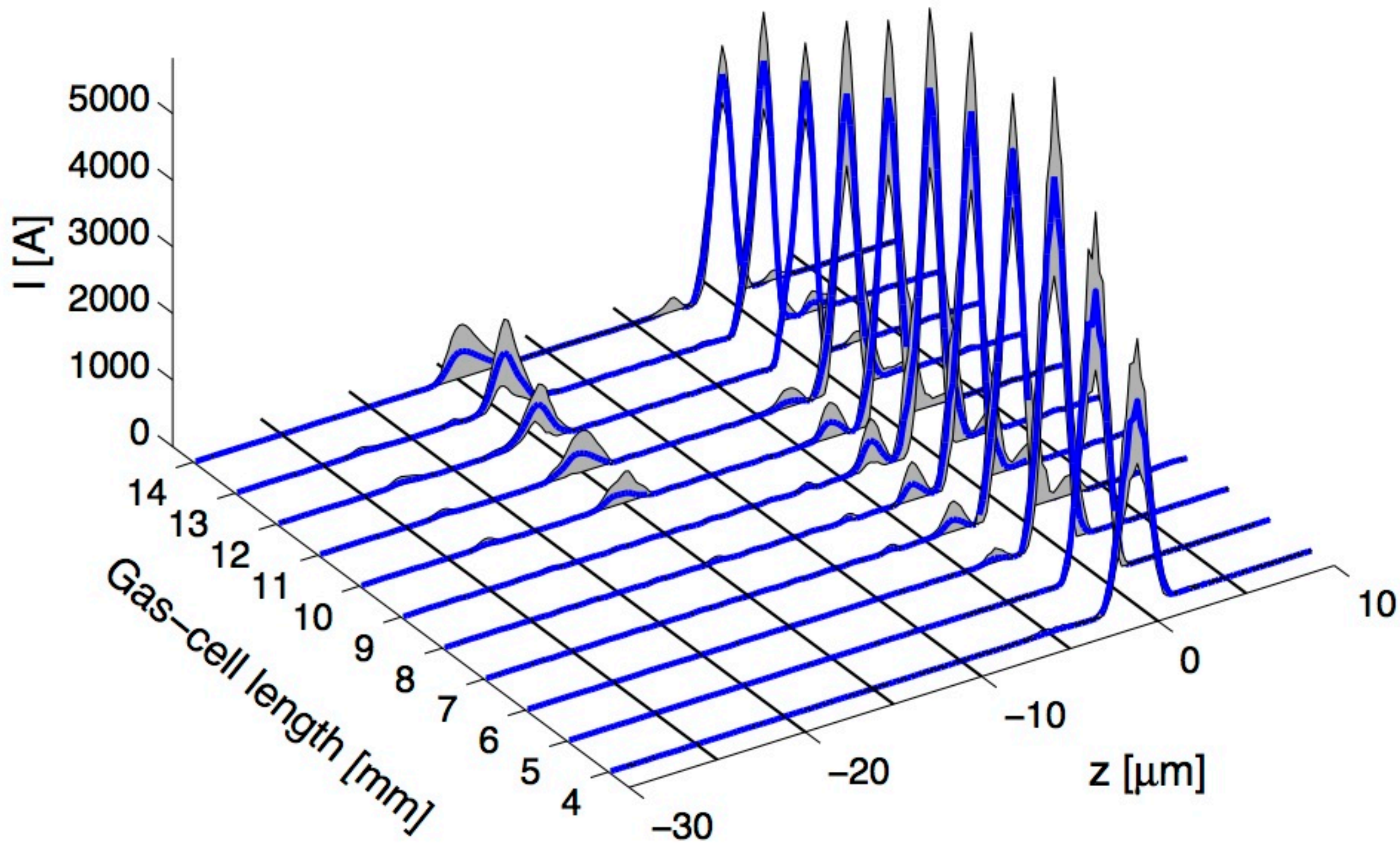
I [A]
5000
4000
3000
2000
1000
0
14
13
12
11
10
9
8
7
6
5
4
Gas–cell length [mm]
–30
–20
–10
0
10
z [µm]

Stable acceleration by forced injection

Colliding pulse injection (J. Faure et al., Nature 444 (2006))

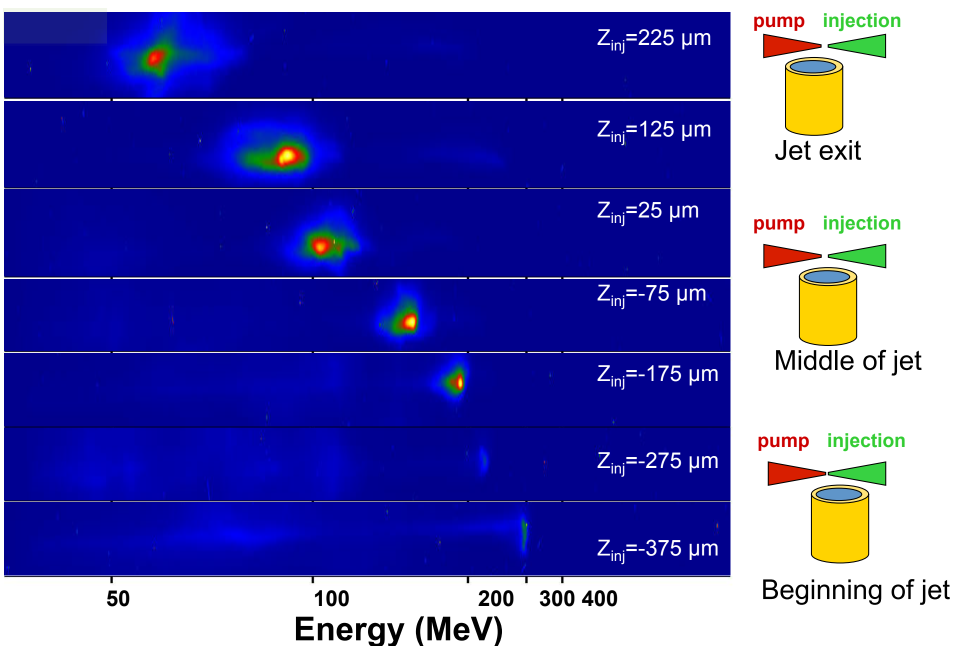

Down-ramp injection (Gonsalves et al., Nat Phys 2071 / DOI:10.1038 (2011))

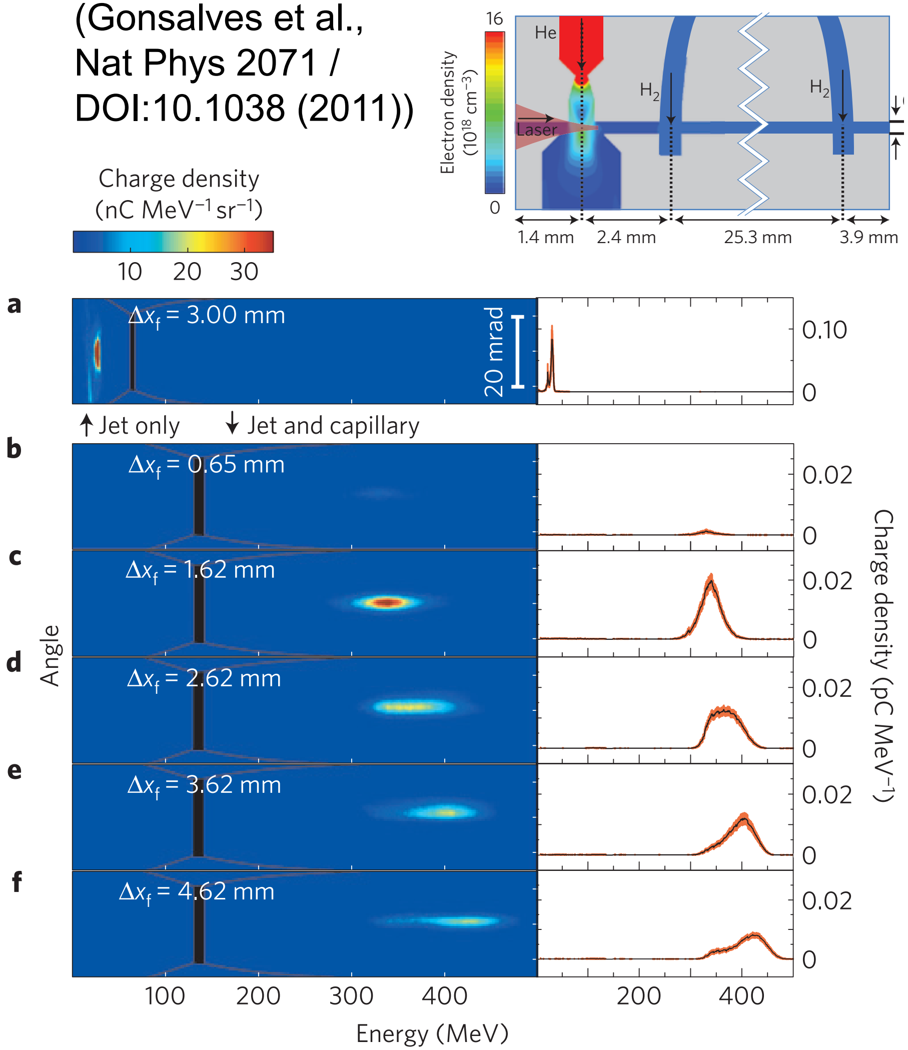

Stable electron acceleration: Shock-front injection into supersonic nozzle

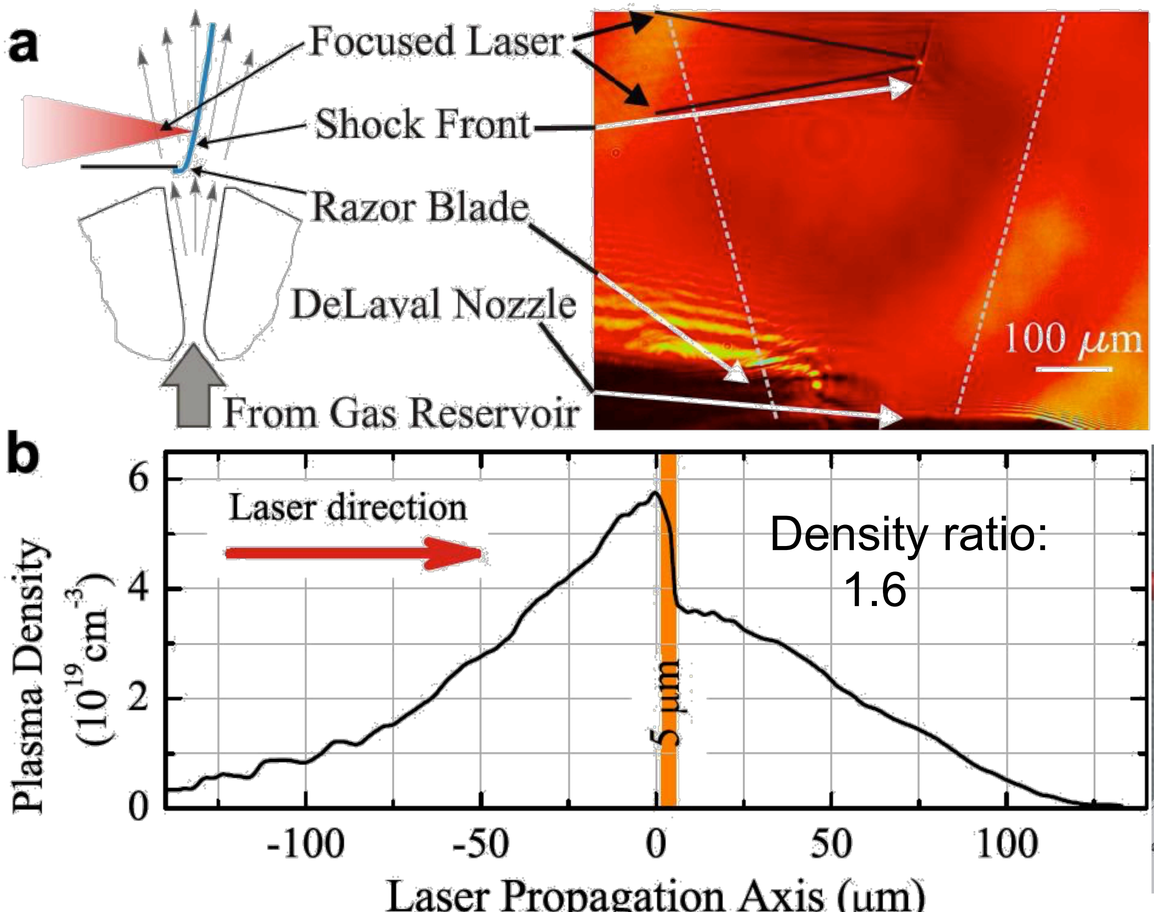

Gas target
supersonic Laval nozzle with 0.75 – 1.5 mm exit diameter

Density ratio: 1.6
Transition: ~ 5 μm
Plasma wavelength: ~ 20 μm

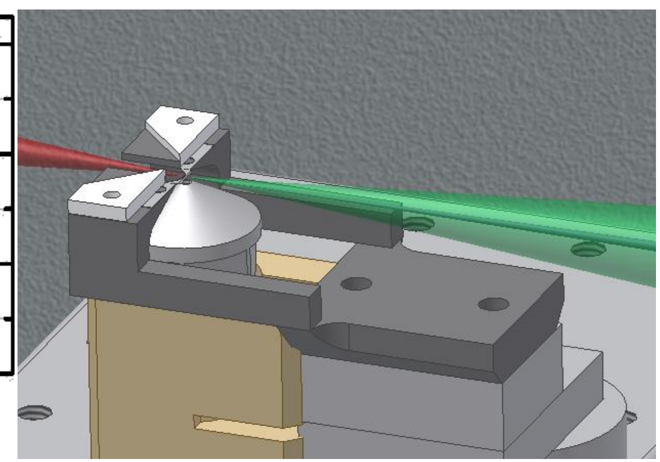

K. Schmid *et al.*, Phys. Rev. Spec. Top. – Acc. Beams, **3**, 091301 (2010)

tuning the electron energy: move blade to move injection point

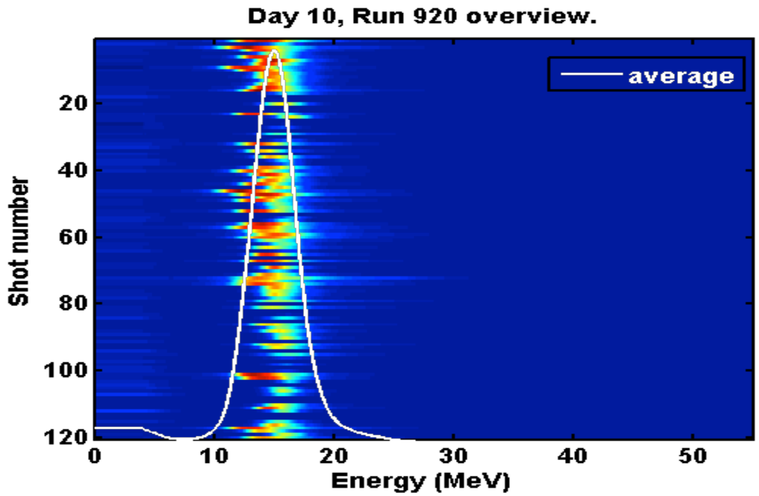

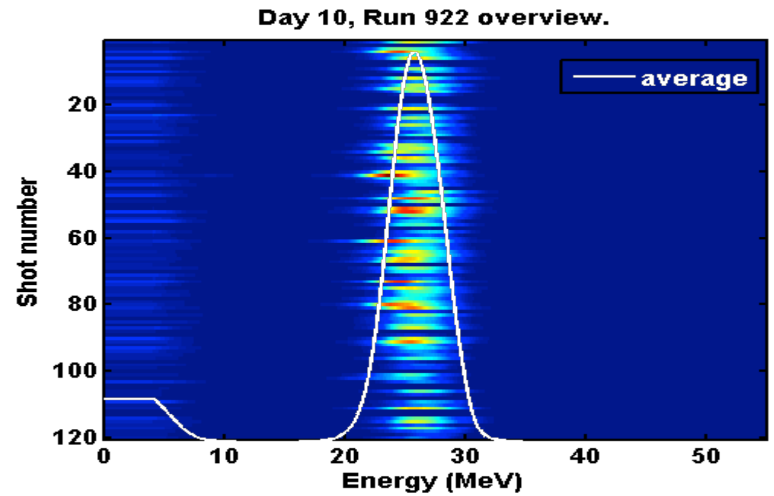

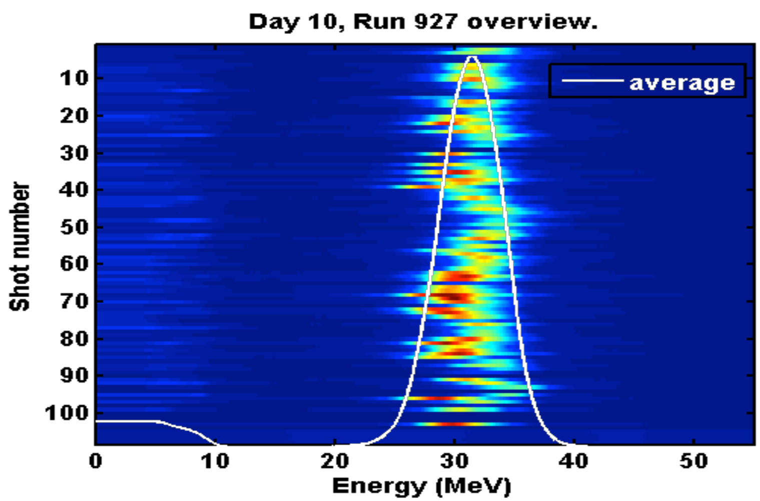

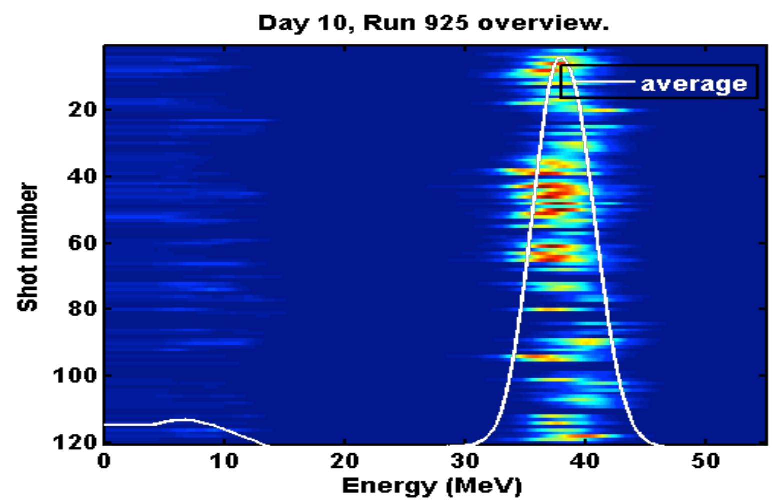

Medium-charge (30-100 pC), low-energy (-100 MeV) beams with narrow energy spread

Ingredient No.2:

Electron deflection

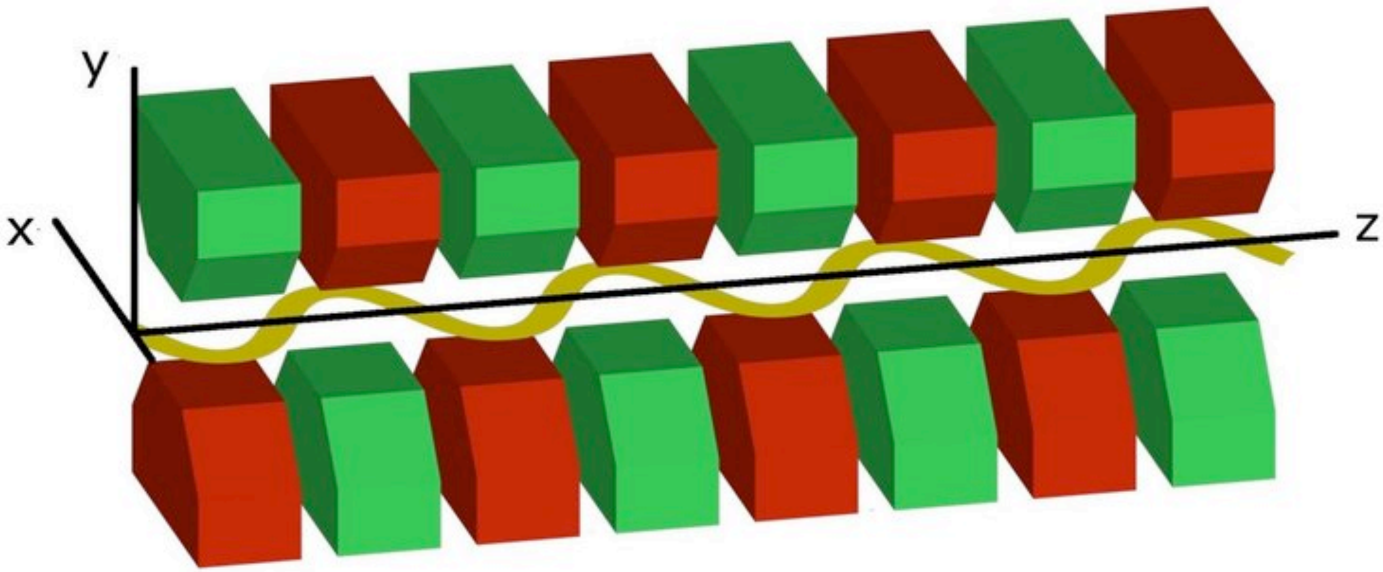

Larmor radiation (see e.g. Jackson) of an accelerated charged particle:

Radiation power: $$P_R = \frac{e^2}{6\pi\varepsilon_0 m_0^2 c^3}\left(\frac{d\vec{p}}{dt}\right)^2$$

Angular distribution: $$\frac{dP_R}{d\Omega} = \frac{e^2}{16\pi^2\varepsilon_0 m_0^2 c^3}\left(\frac{d\vec{p}}{dt}\right)^2 \sin^2\Psi$$ (Hertzian dipole)

Find relativistic invariant form of Larmor formula:

Transform time: $dt \to d\tau = \frac{1}{\gamma}dt$ and four-momentum: $\left(\frac{dP_\mu}{d\tau}\right)^2 \to \left(\frac{d\vec{p}}{d\tau}\right)^2 - \frac{1}{c^2}\left(\frac{dE}{d\tau}\right)^2$

$$P_R = \frac{e^2 c}{6\pi\varepsilon_0\left(m_0 c^2\right)^2}\left[\left(\frac{d\vec{p}}{d\tau}\right)^2 - \frac{1}{c^2}\left(\frac{dE}{d\tau}\right)^2\right]$$

Deflection in magnetic field: *ΔE/dt*=0

$$P_R = \frac{e^2 c}{6\pi\varepsilon_0 \left(m_0 c^2\right)^2} \left(\frac{dp}{d\tau}\right)^2 = \frac{e^2 c \gamma^2}{6\pi\varepsilon_0 \left(m_0 c^2\right)^2} \left(\frac{dp}{dt}\right)^2$$

$$\frac{dp}{dt} = p\omega = p\frac{v}{R}; \quad E = pc; \quad \gamma = \frac{E}{m_0 c^2}$$

$$P_R = \frac{e^2 c}{6\pi\varepsilon_0 \left(m_0 c^2\right)^4} \frac{E^4}{R^2}$$

average rest frame:

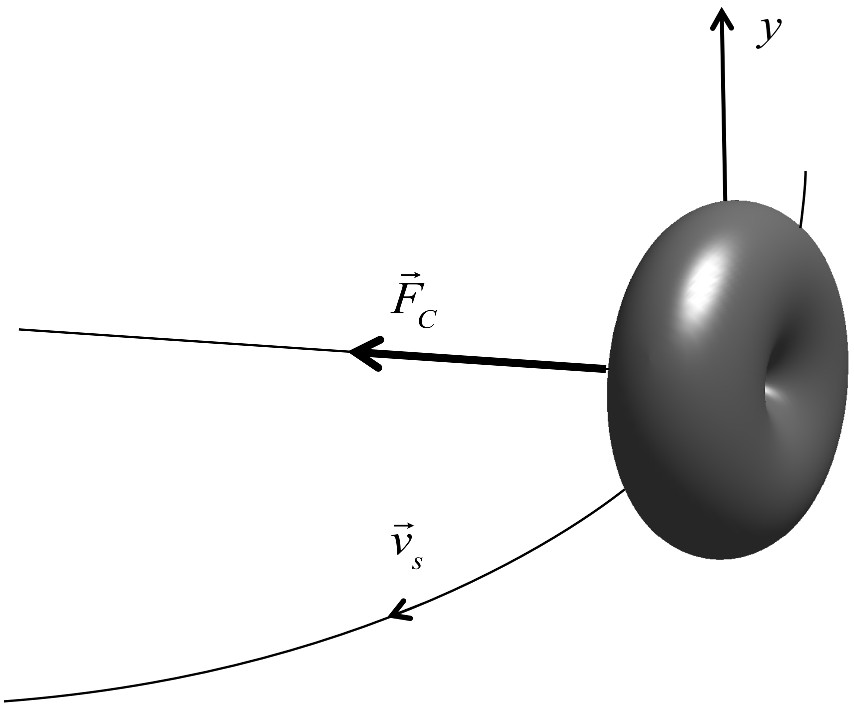

lab frame:

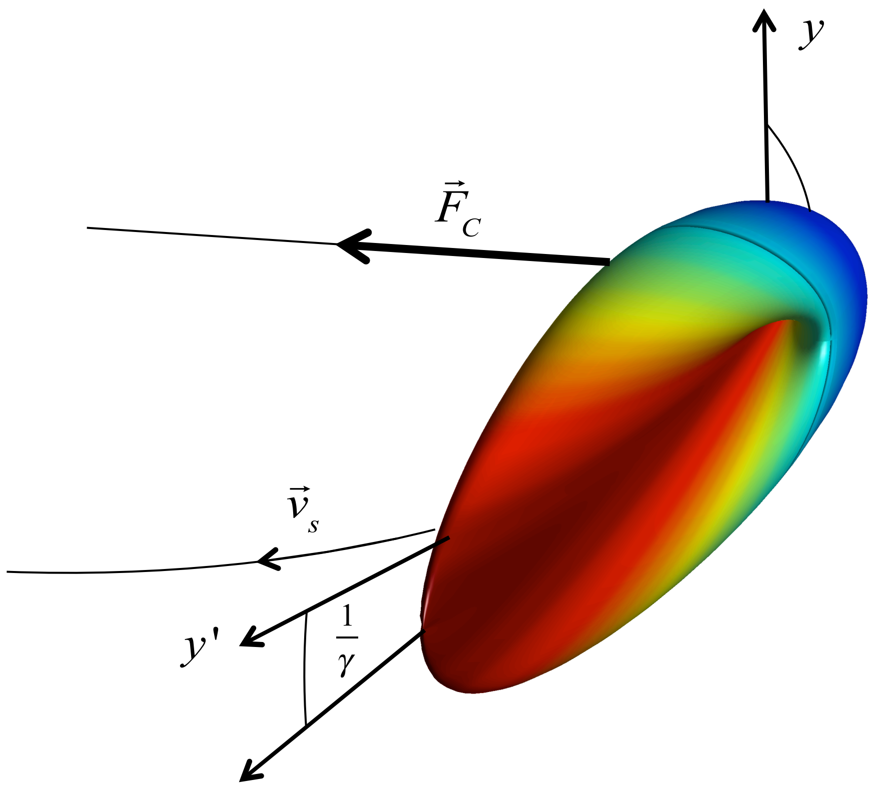

spontaneous synchrotron radiation spectrum:

radiation beam sweeps past observer during $\Delta t = \frac{2R}{c\beta}\frac{1}{\gamma} - \frac{2R}{c}\sin(1/\gamma) = t_e - t_\gamma \approx \frac{4R}{3c\gamma^3}$

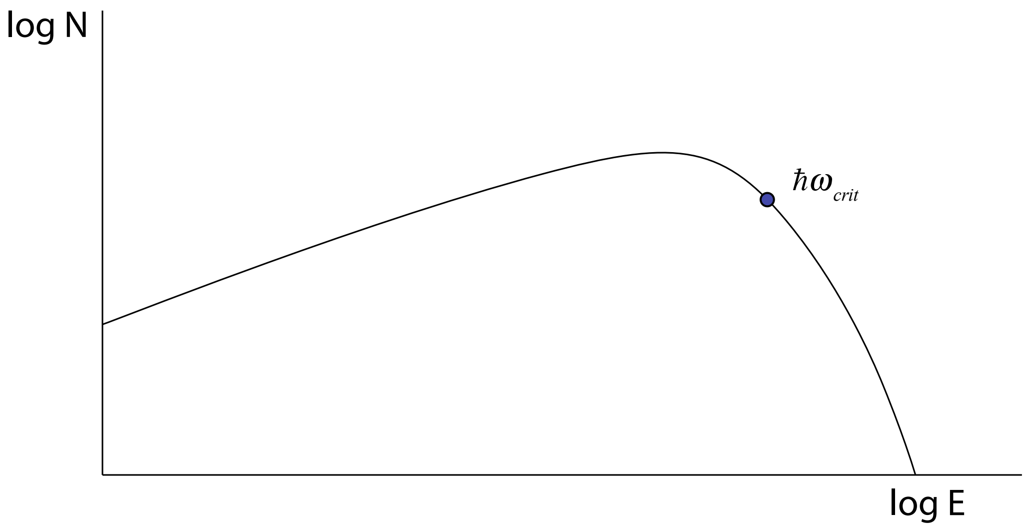

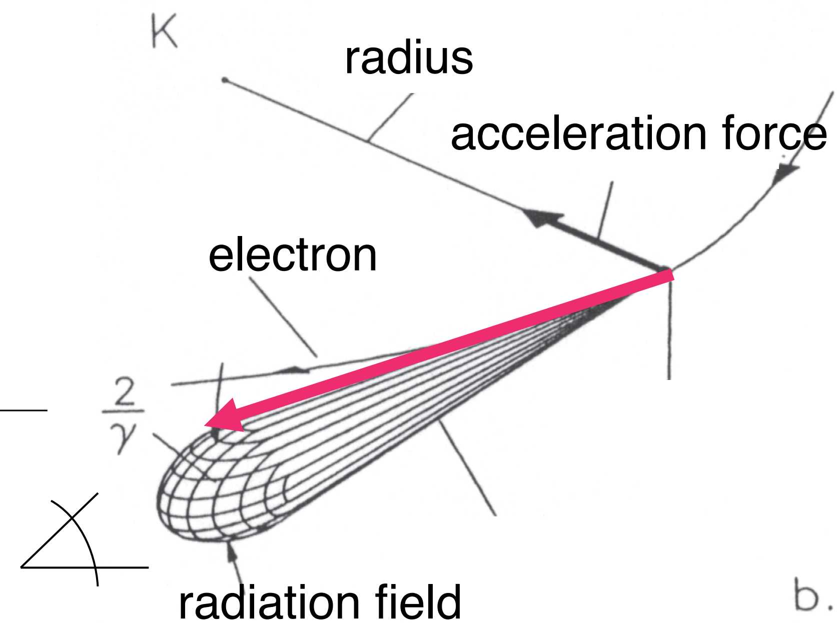

...which leads to a critical radiation frequency

$$\omega_{crit} = \frac{2}{\Delta t} = \frac{3c\gamma^3}{2R}$$

and a spectral energy density: $$\frac{d\dot{N}}{d\varepsilon/\varepsilon} = \frac{3\sqrt{3}e\gamma^4 I_b}{8\pi\varepsilon_0 R\omega_c\hbar}\xi\int_\xi^\infty K_{5/3}(\xi)\,d\xi, \qquad \xi = \frac{\omega}{\omega_{crit}}$$

periodic deflection:

“identical“ emission at each turning point

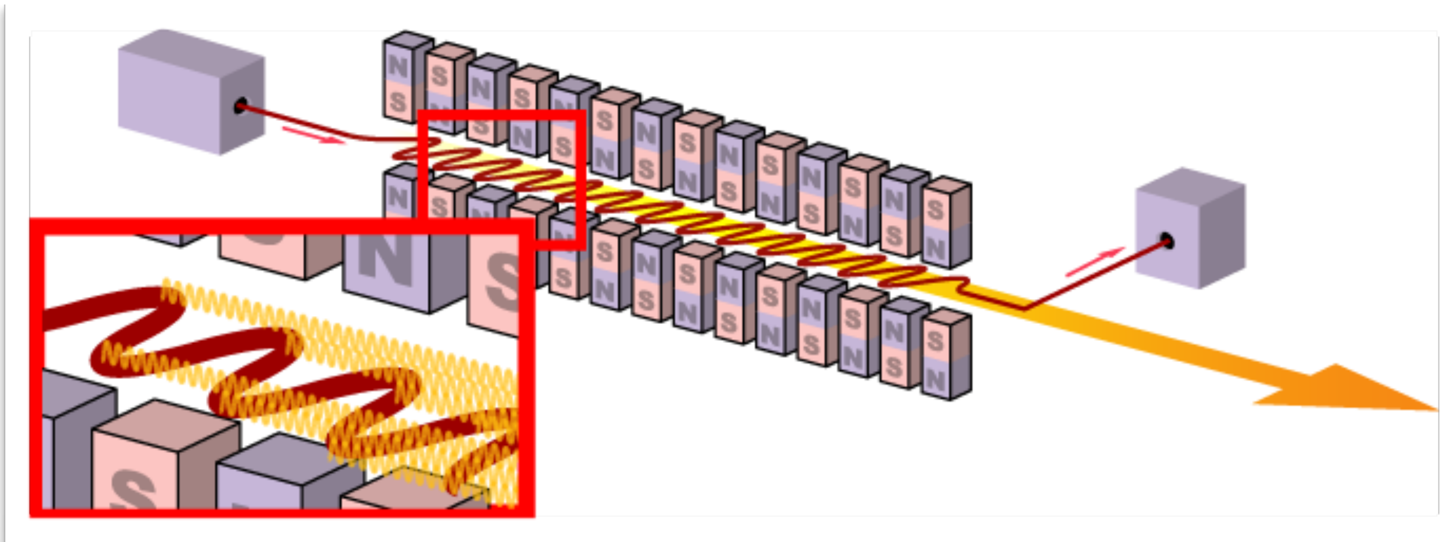

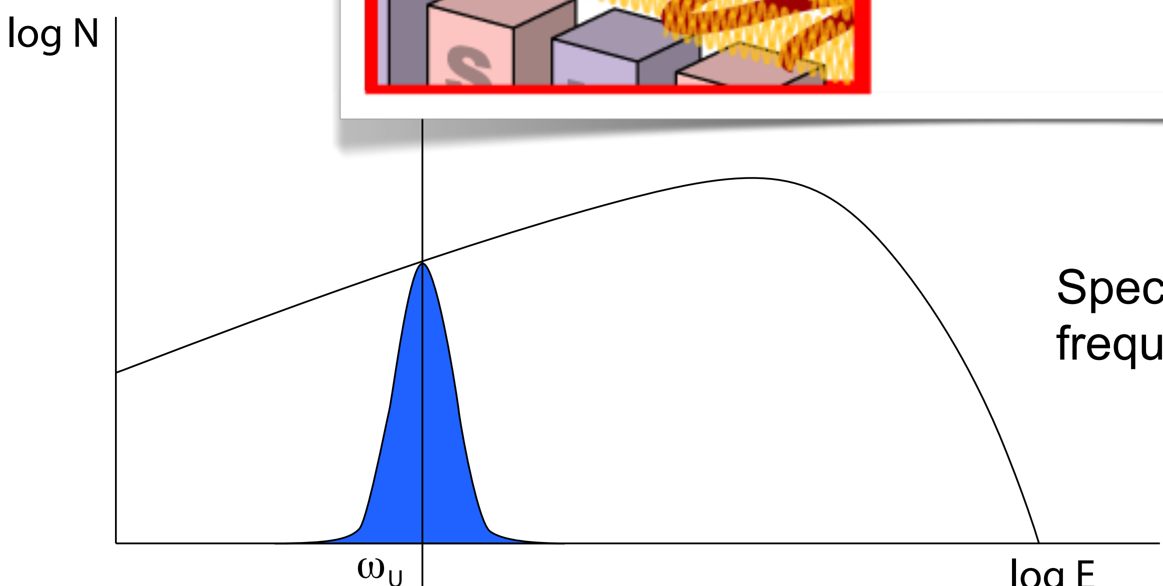

Spectrum is enhanced at wiggling frequency!

Wiggling wavelength

Instantaneous field amplitude

$$\lambda_{x-ray} = \frac{\lambda_{u,b,l}}{2(4^{*})\gamma^{2}}\left(1 + \frac{a_0^2}{2} + \gamma^2\theta^2\right)$$

Electron gamma factor

Observation angle range

X-ray spectrum is influenced by:

- Electron energy and bandwidth
- Wiggling field strength and number of oscillations
- Observation direction and solid angle
- Wiggling period

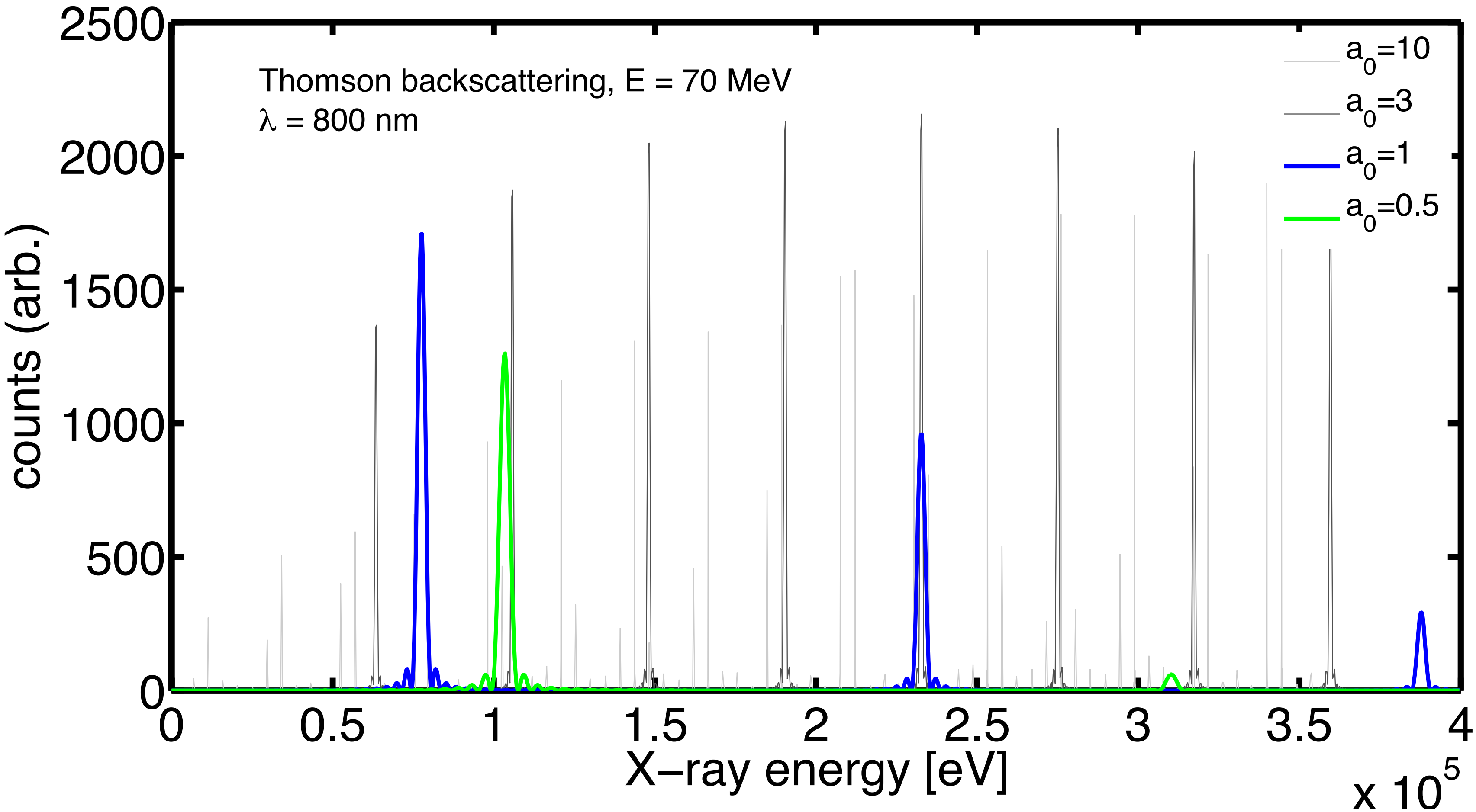

Collimated, monochromatic e-beam, 25 period, flat-top optical undulator

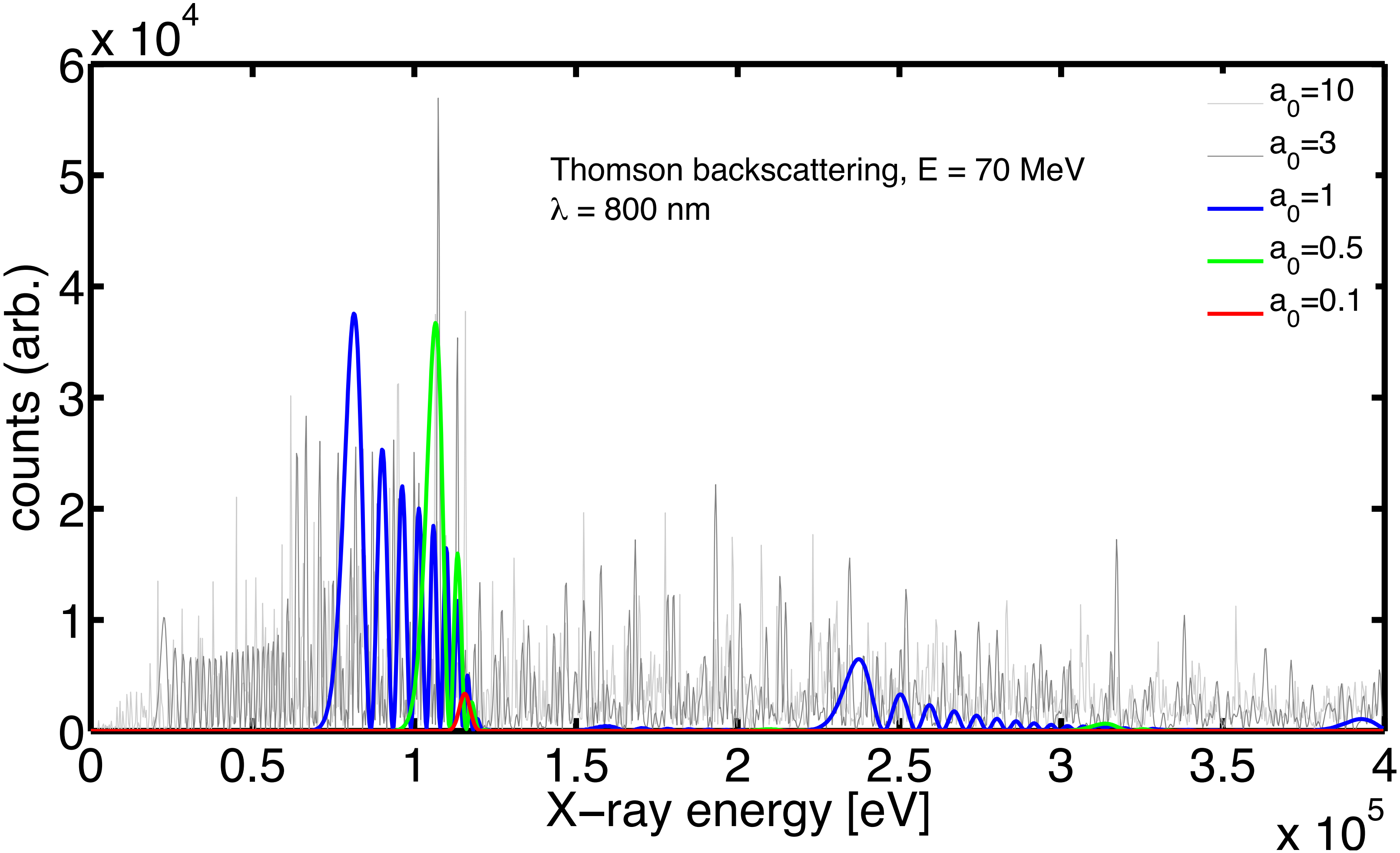

Collimated, monochromatic e-beam, 30 fs laser pulse

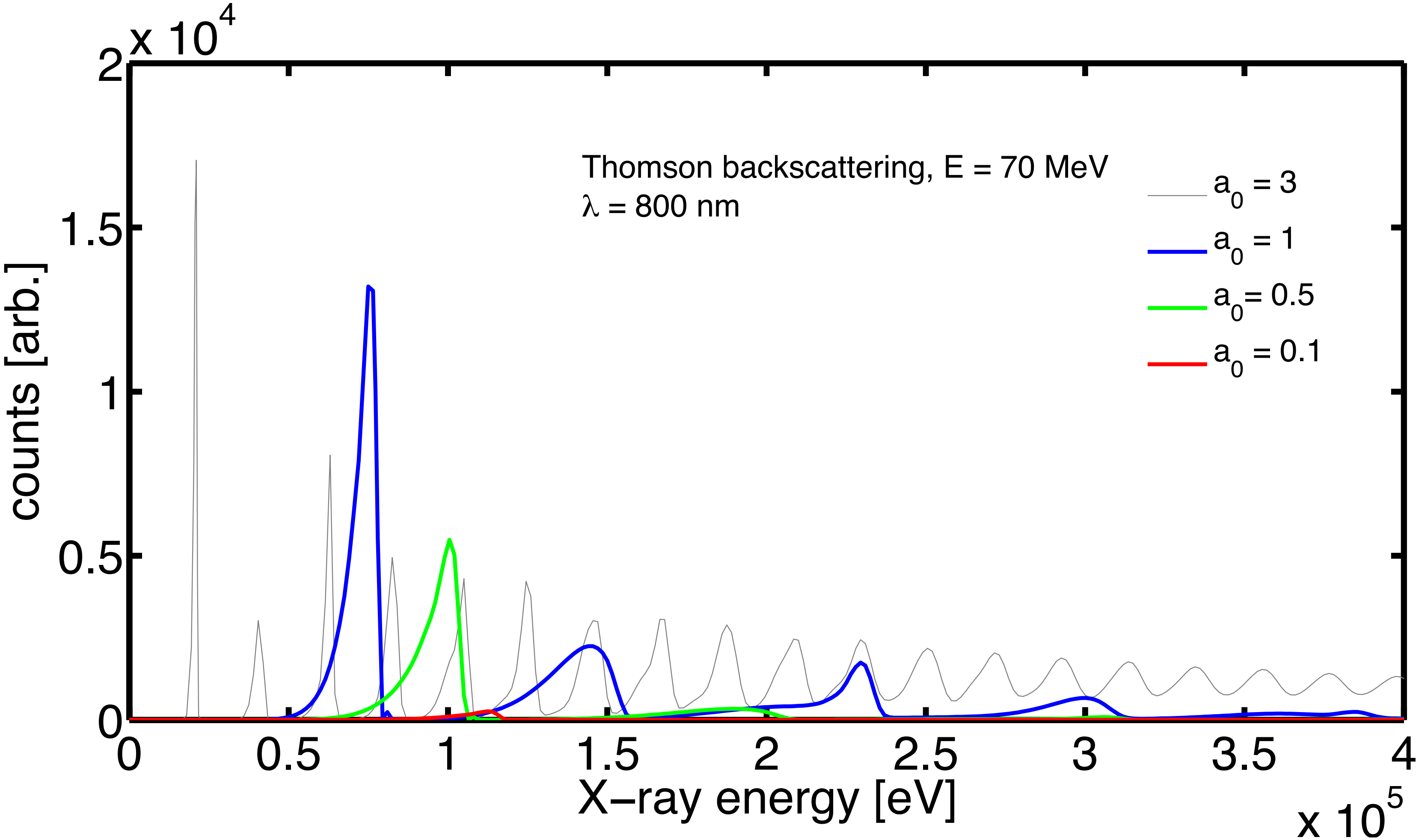

Divergent (2.2 mrad), monochromatic e-beam, 25 period, flat-top optical undulator

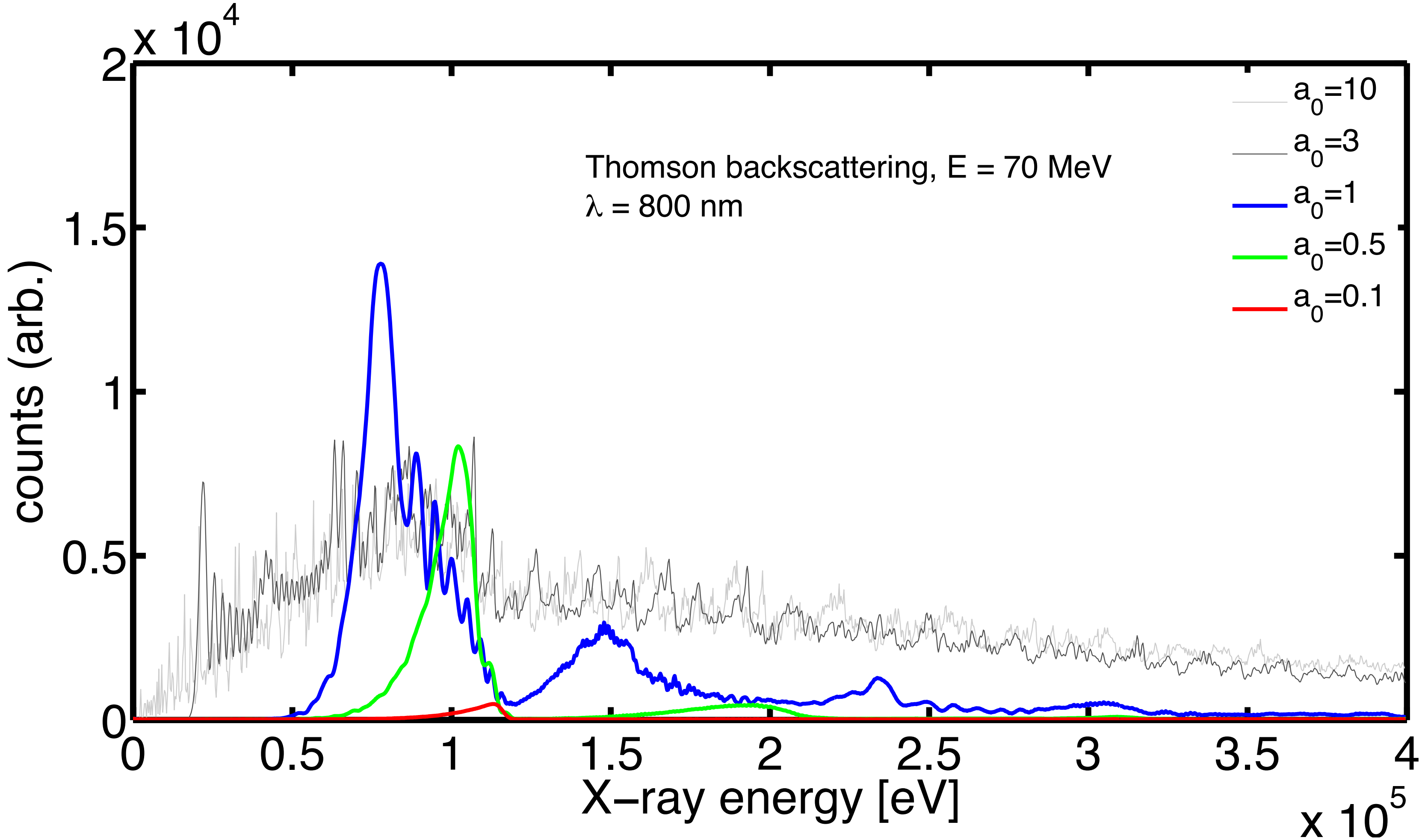

Divergent, monochromatic e-beam, 30 fs laser pulse

Undulator radiation

In collaboration with:

F. Grüner Group (HHU)
U. Kleineberg Group (LMU)

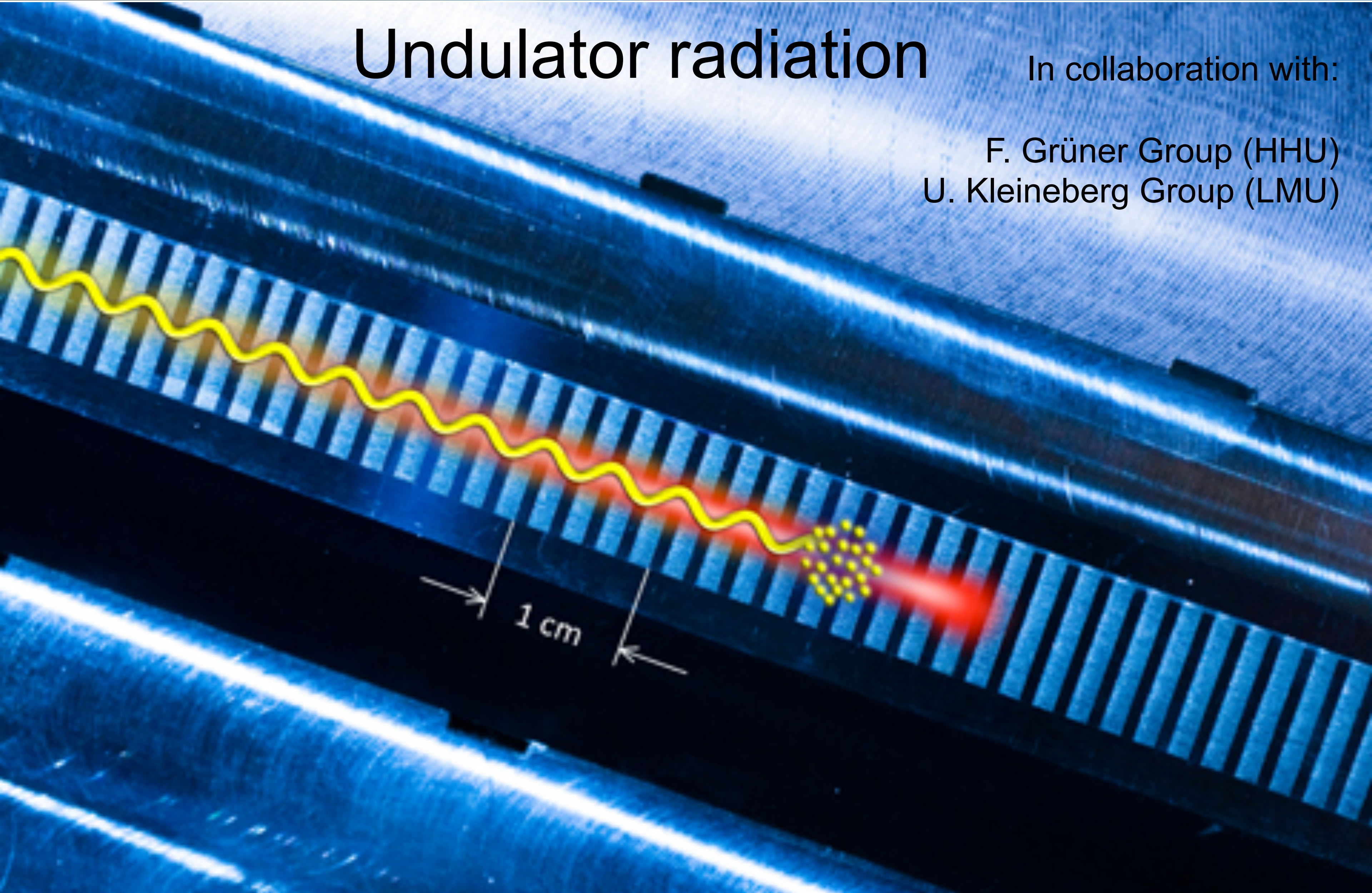

1. Undulator radiation (with F.Grüner et al. & Kleineberg et al.)

Electron spectra:

ATLAS 60

1. 5 J on target, 26 fs
~500 MeV peak energy
~100 pC total charge

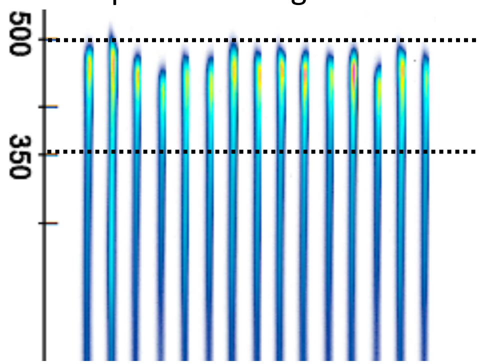

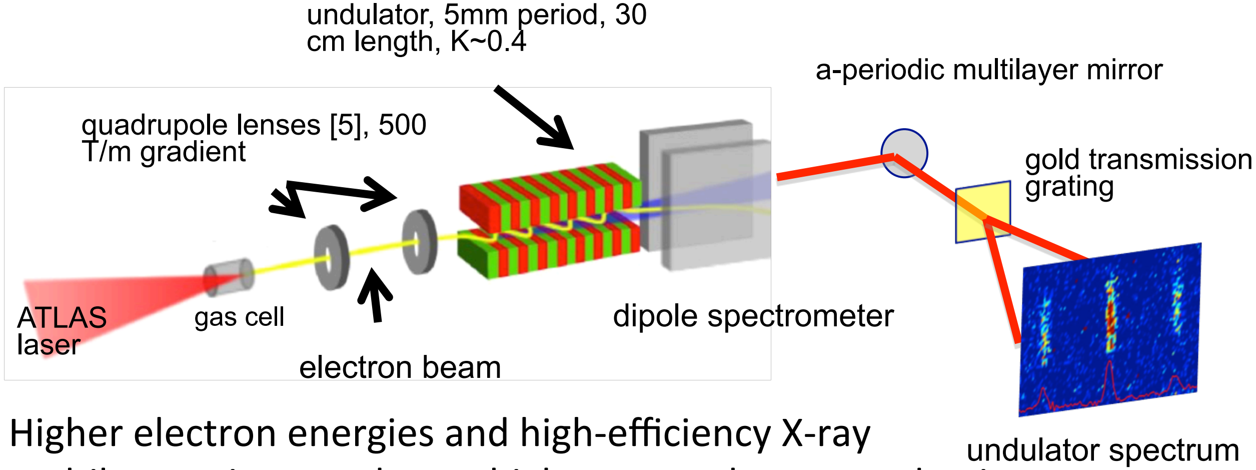

Higher electron energies and high-efficiency X-ray multilayer mirrors enhance high-energy photon production

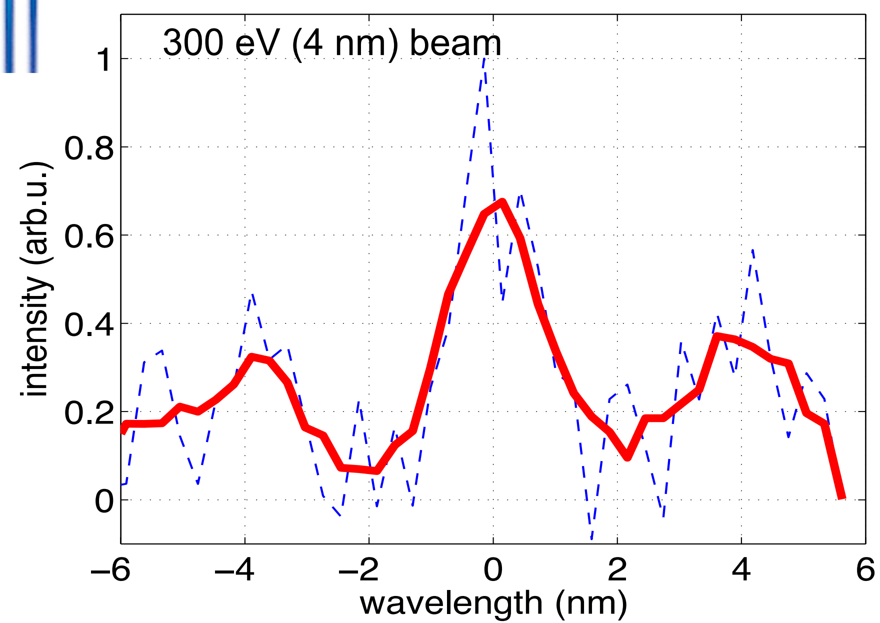

- Requires multi-GeV electrons to reach energy range for human diagnosis.
- May become valuable source radiation biology studies

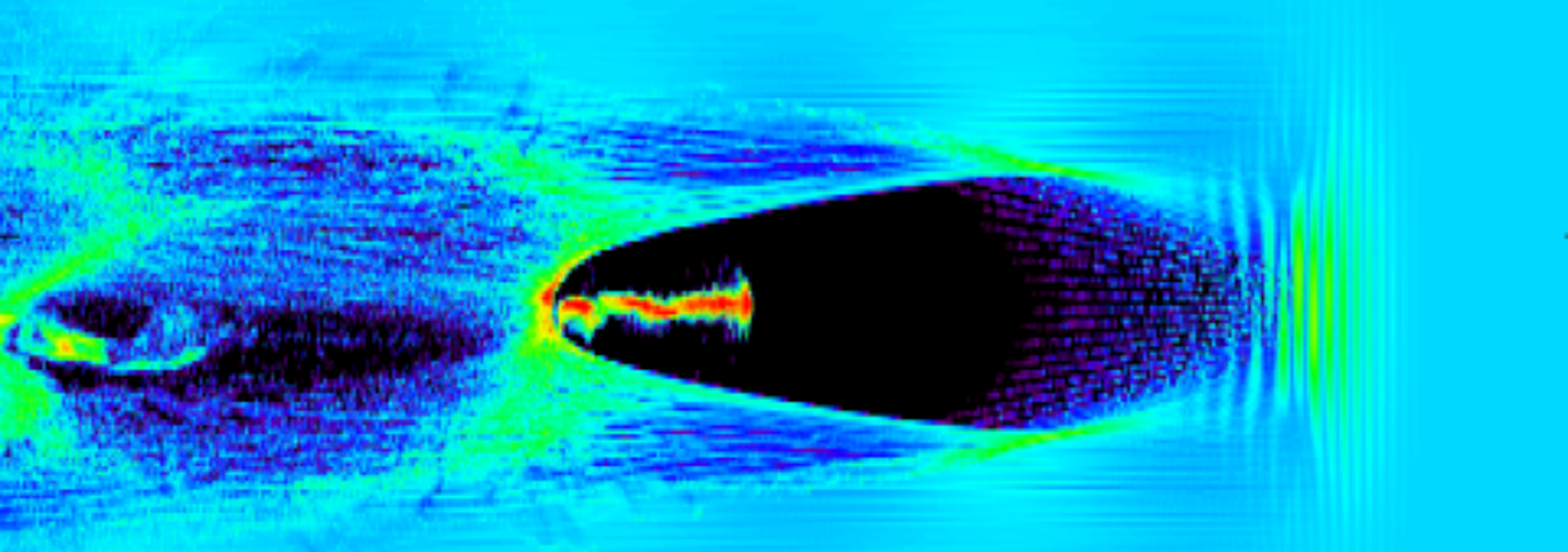

2
Betatron radiation

Betatron emission

$$\lambda_{x-ray} = \frac{1}{3K\gamma^2}\lambda_\beta, \quad \lambda_\beta \approx \sqrt{2\gamma}\lambda_p \approx 300\ \mu\text{m}$$

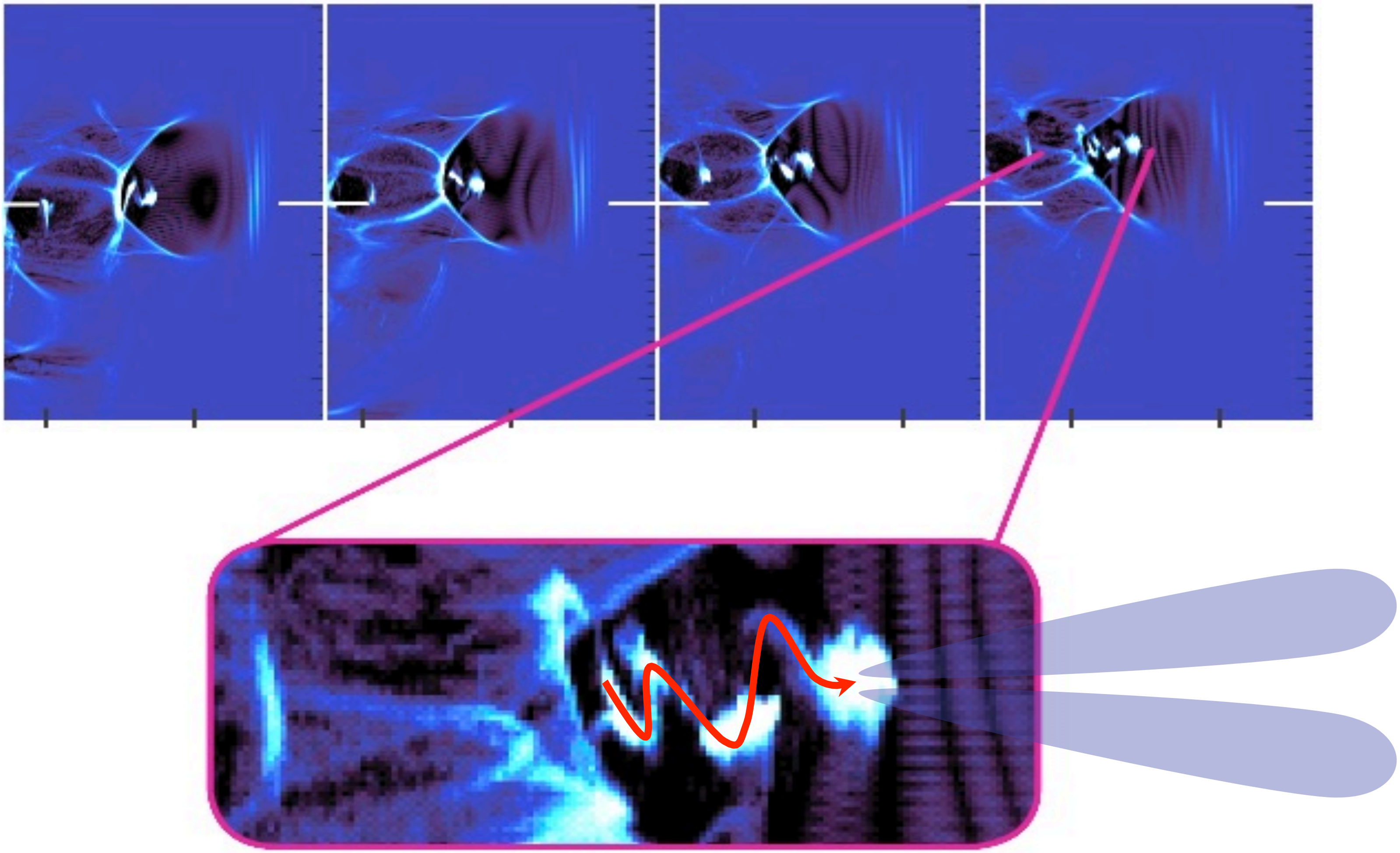

Perspectives

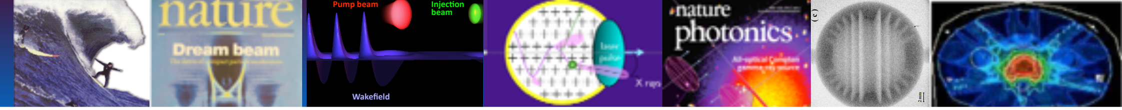

Results extremely important for :

Designing future accelerators
Compact X ray source (Thomson, Compton, Betatron, or FEL)
Applications (chemistry, radiotherapy, medicine, material science, ultrafast phenomena studies, etc...)

First X rays betatron contrast images

S. Fourmaux *et al.*, Opt. Lett. **36**, 13 (2011)

S. Kneip *et al.*, Appl. Phys. Lett. **99**, 093701 (2011)

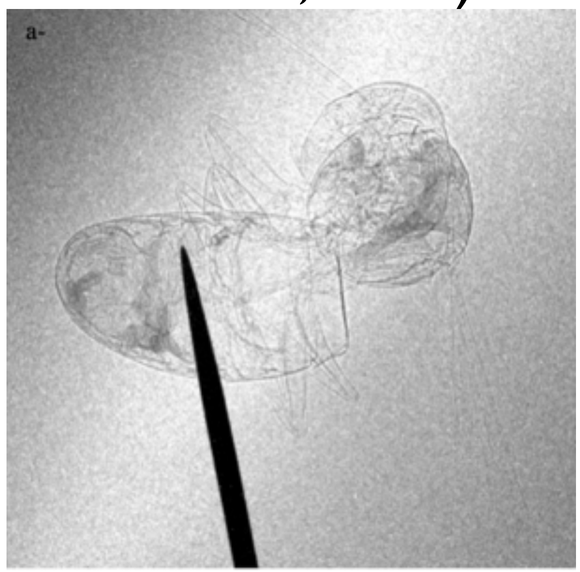

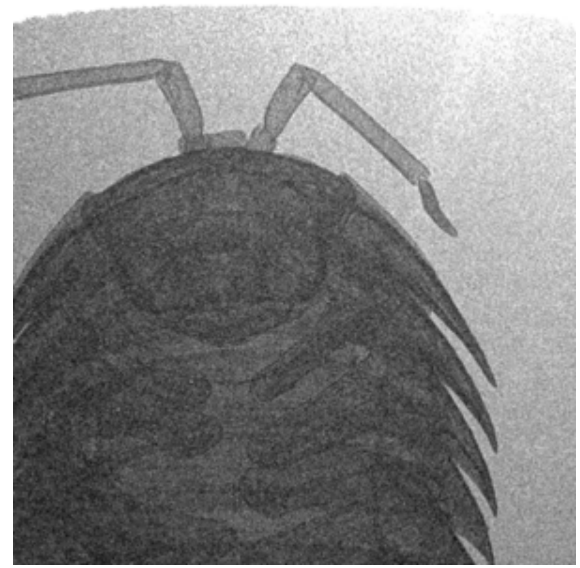

Courtesy of K. Krushelnick

V. Malka *et al.*, Nature Physics **4** (2008)
E. Esarey et al. , Rev. Mod. Phys. **81**, 1229 (2009)
S. Corde et al., Rev. of Modern Physics **85**, 1 (2013)

Are these beams any good for applications?
Single-shot phase contrast imaging

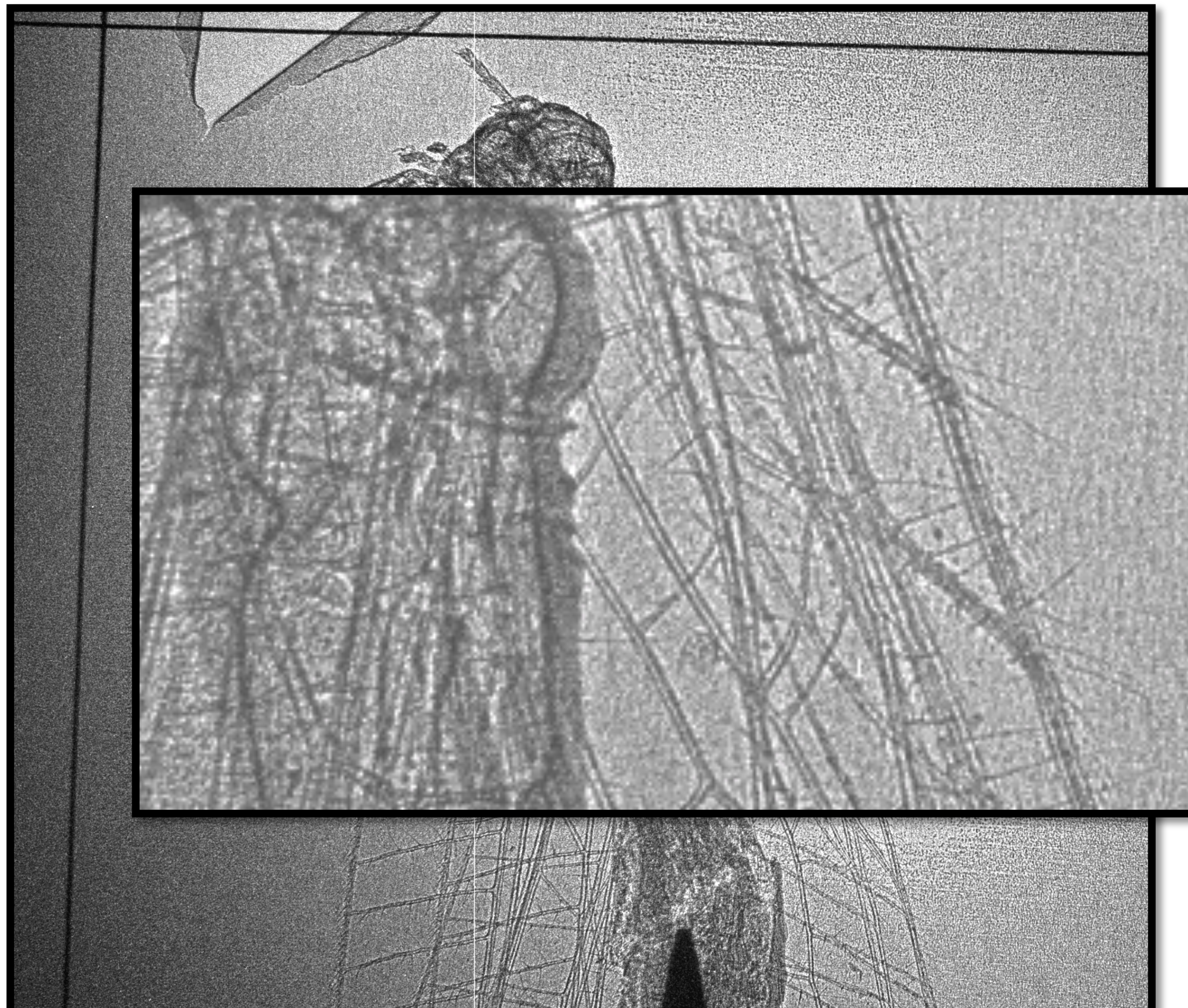

Betatron radiation source characteristics

spectrum

source size

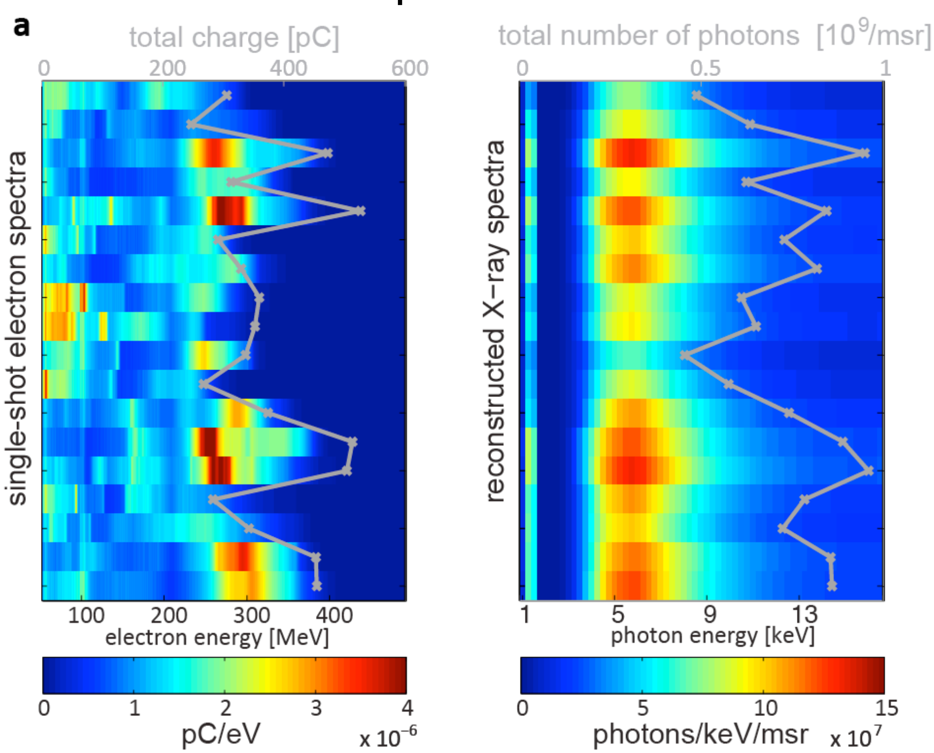

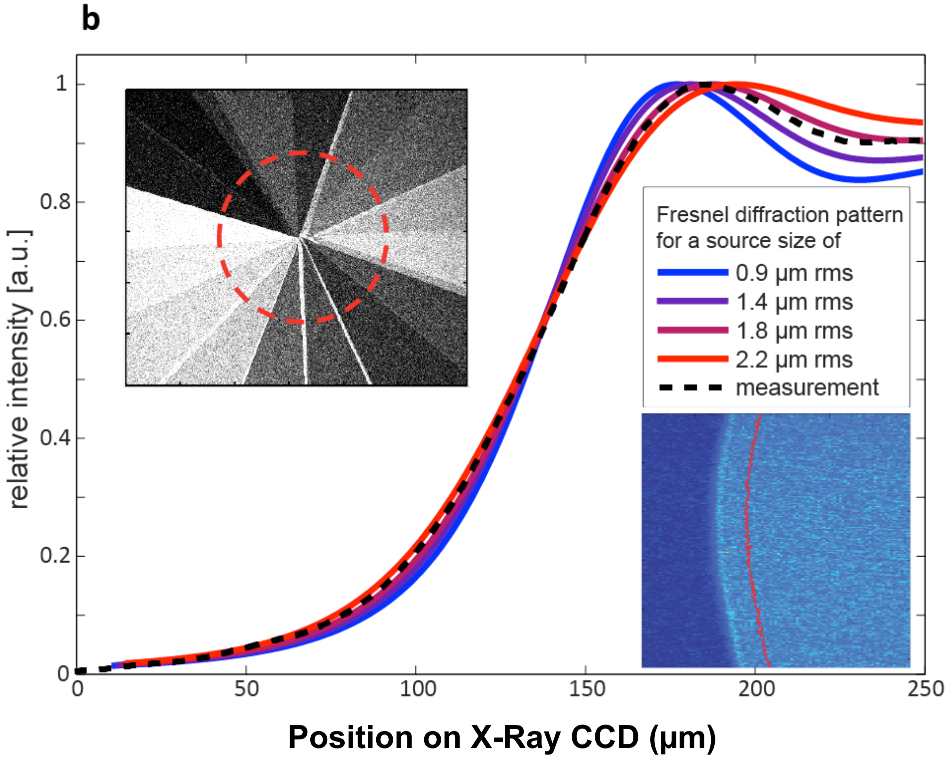

peaks at 5.5 KeV

best fit 1.7 μm

assuming a 5-fs pulse duration, this infers a peak brilliance of
2×10^{22} ph/($s^2 mm^2 mrad^2$ 0.1% bandwidth)

Tomography: Line projections and Radon transform:

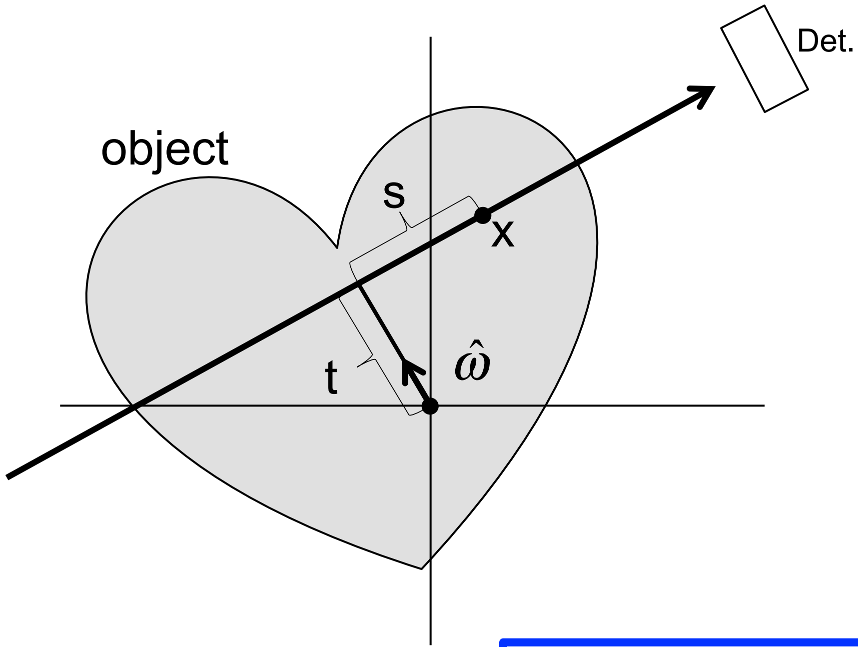

Parametrize each point on ray by a direction unit vector ω, distance to rotation center t and longitudinal position s:

$$f\left(\vec{x}\right) = f\left(\vec{\omega}t + s\vec{\omega}^{\perp}\right)$$

Then the Radon transform yields a representation of the object function f in the variables t and ω:

$$Rf\left(t,\omega\right) = \int_{x\cdot\omega=t} f(x)\,dx = \int_{-\infty}^{\infty} f\left(\vec{\omega}t + s\vec{\omega}^{\perp}\right)ds$$

Tomography:

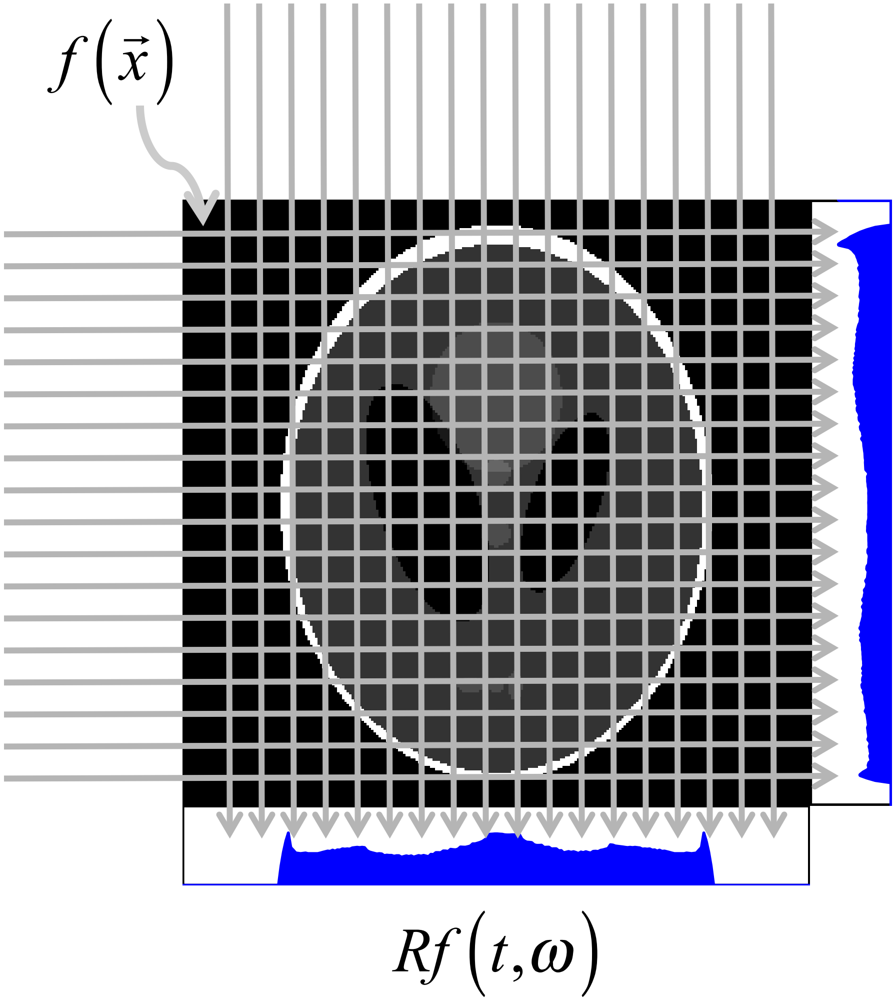

- Projections are (n-1)-dim. distribution functions representing the line integrals of the n-dim. density distribution along each ray path.
- The set of projections under different angles α constitute a sinogram:

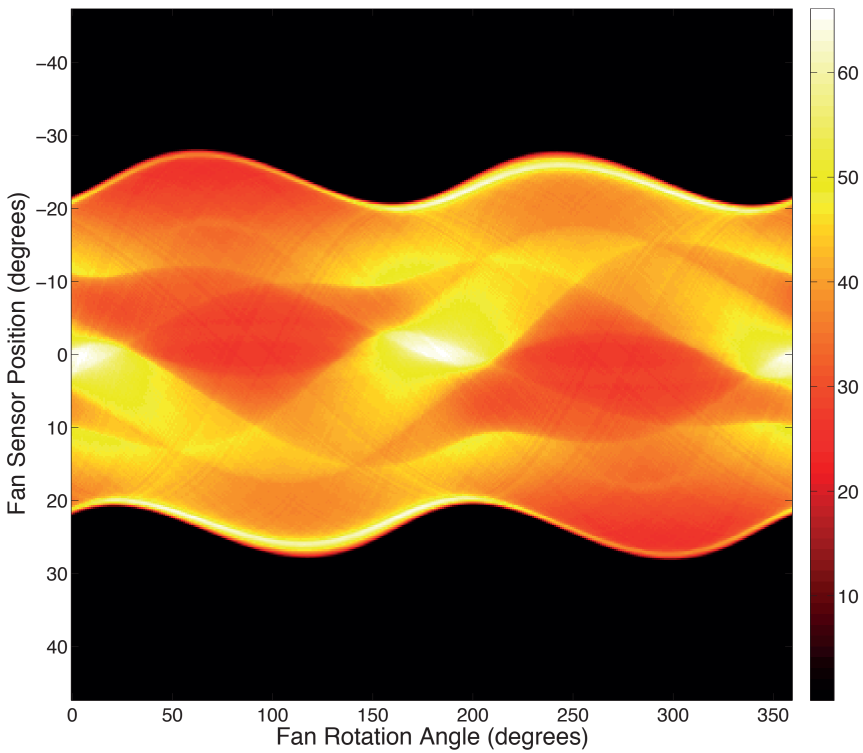

Reconstruction: Inversion of Radon transform: Overlapping backprojections

2 angles

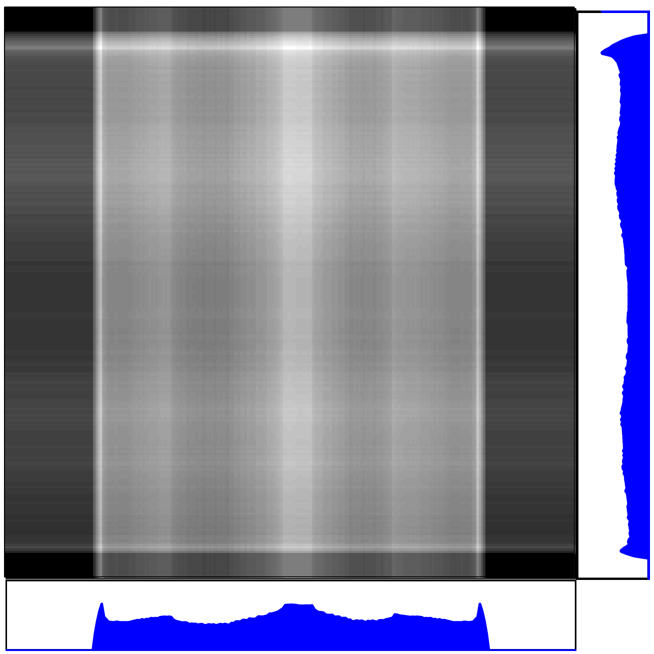

360 angles

Filtered backprojection formula:

$$f = \frac{1}{4\pi} R^{\#} H \frac{d}{dt}\left(Rf\right)$$

filter

backproj. operator

Hilbert transform

$$H\left(y\right) = \frac{1}{\pi} \int_{-\infty}^{\infty} \frac{f\left(x\right)}{y-x} dx$$

propagation-based phase-contrast imaging

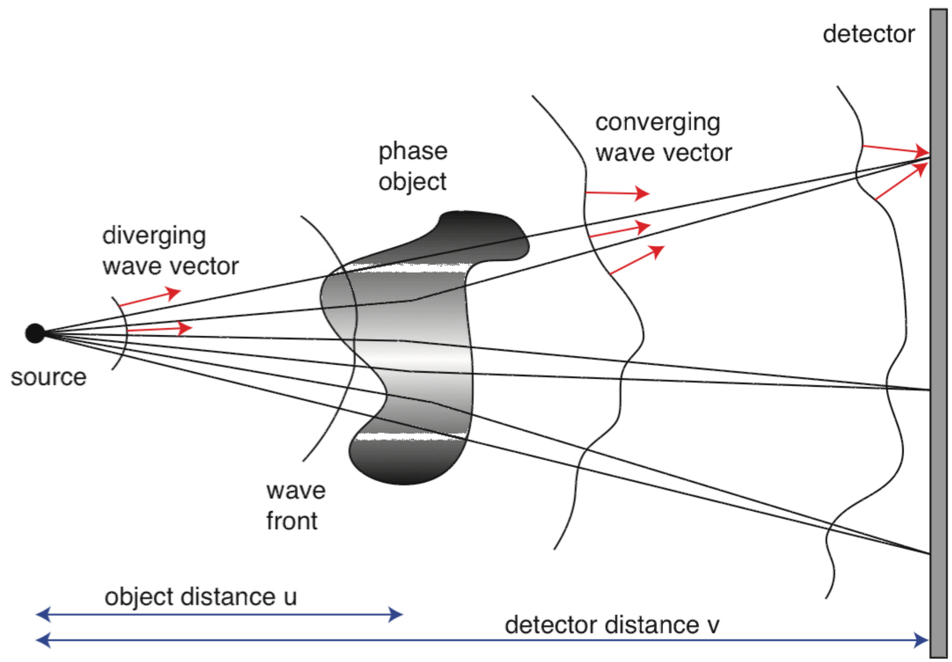

The intensity distribution on the detector is a result of wavefront distortions introduced by phase object. The Transport of Intensity Equation relates sample thickness to measured intensity distribution:

$$T\left(\vec{r}\right) = -\frac{1}{\mu_{poly}} \times ln\left(F^{-1}\left\{\frac{\frac{F(I(M\vec{r}))}{I_0}}{1+\frac{R\delta_{poly}}{M\mu_{poly}}\left|\vec{k}\right|^2}\right\}\right)$$

The transport-of intensity-equation (TIE) relates the edge-enhanced image at the detector (a) to the phase map of the insect (b)

$$T\left(\vec{r}\right) = -\frac{1}{\mu_{poly}} \times ln\left(F^{-1}\left\{\frac{\frac{F(I(M\vec{r}))}{I_0}}{1+\frac{R\delta_{poly}}{M\mu_{poly}}\left|\vec{k}\right|^2}\right\}\right)$$

tomographic reconstruction of 2-D projections yields cuts through sample (edge anhancement (a) and phase images (b,c))

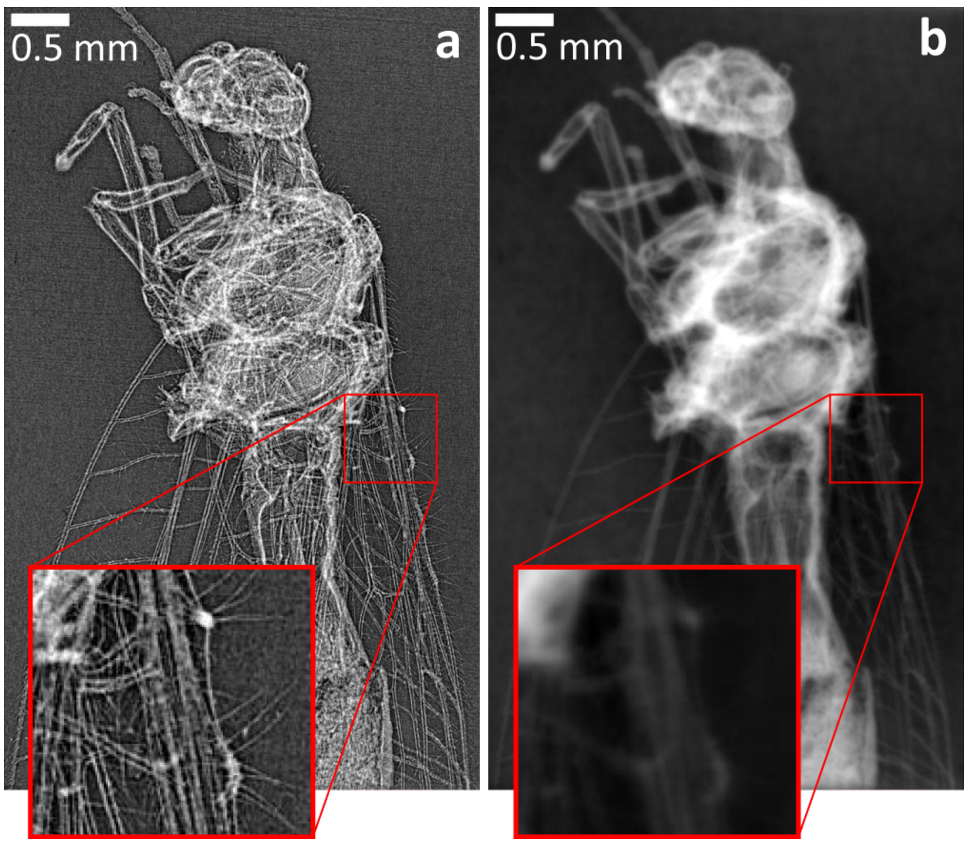

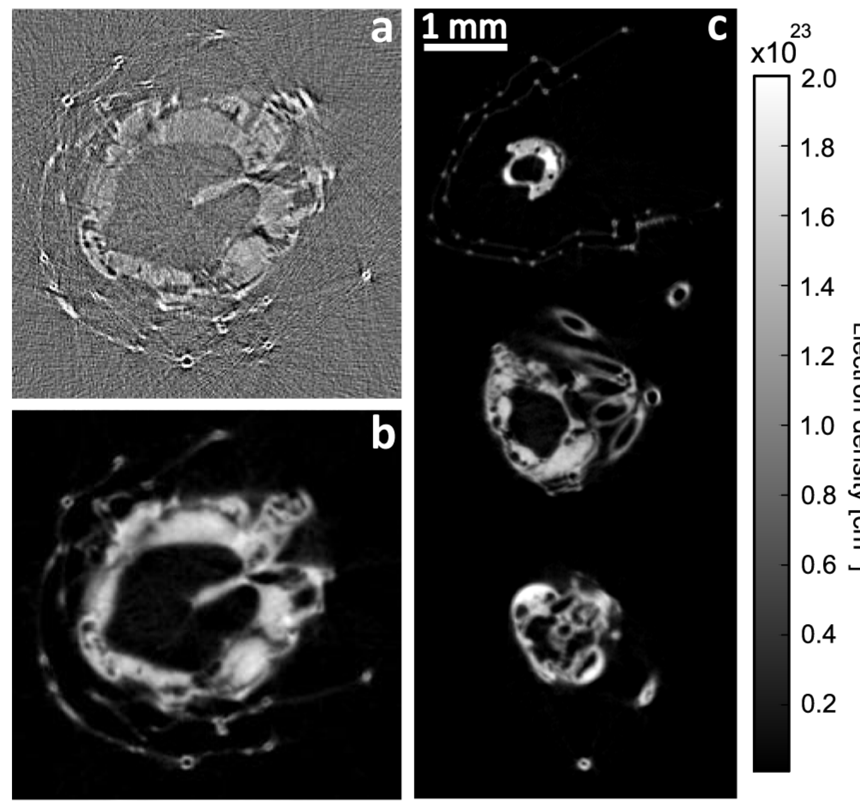

3D rendering of the fly (with S. Schleede, F. Pfeiffer et al., TUM)

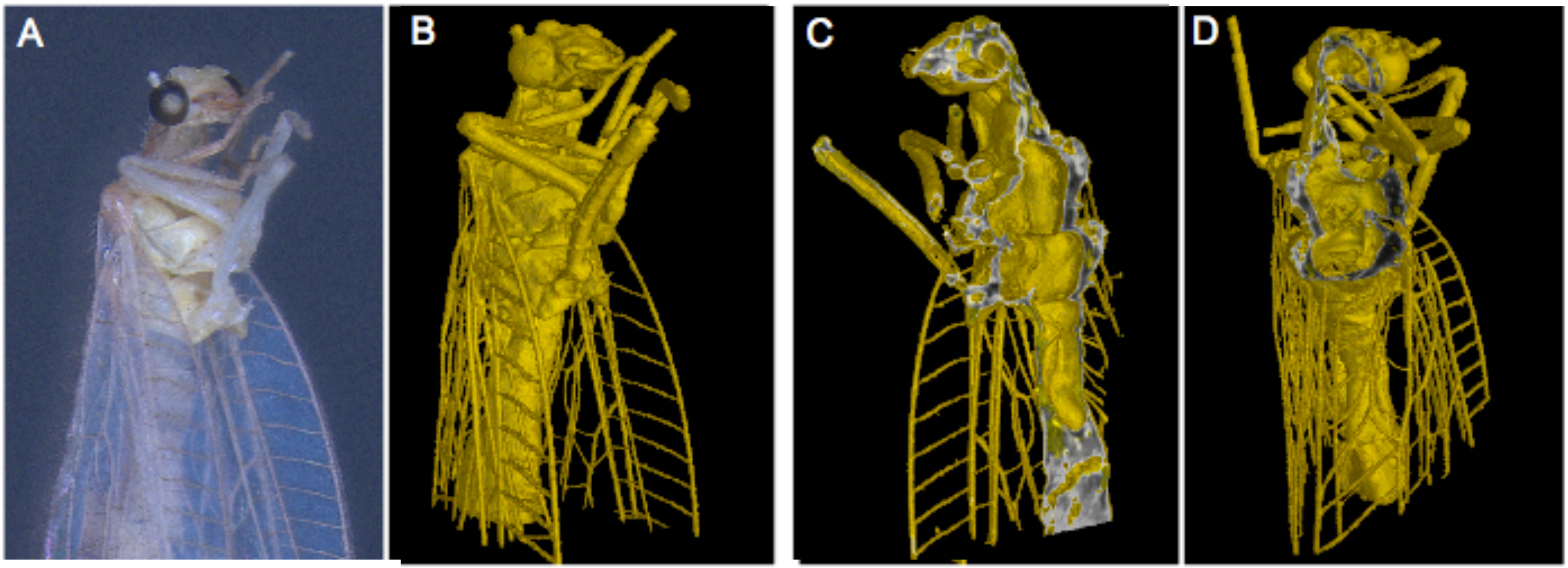

J. Wenz et al., submitted to Nat. Photonics

- Demostrates suitability for high-resolution imaging (well below 1 mm) for an all-optical source
- Photon energies for human diagnosis require 10J-class laser, long scan times.

Bone Tomography

by courtesy of S.P.D. Mangles

- Trabecular/cancellous bone - intricate spongy internal structure
- Efficient distribution of mechanical stress throughout bone volume
- Very high surface area to volume ratio – site of intense bone remodelling

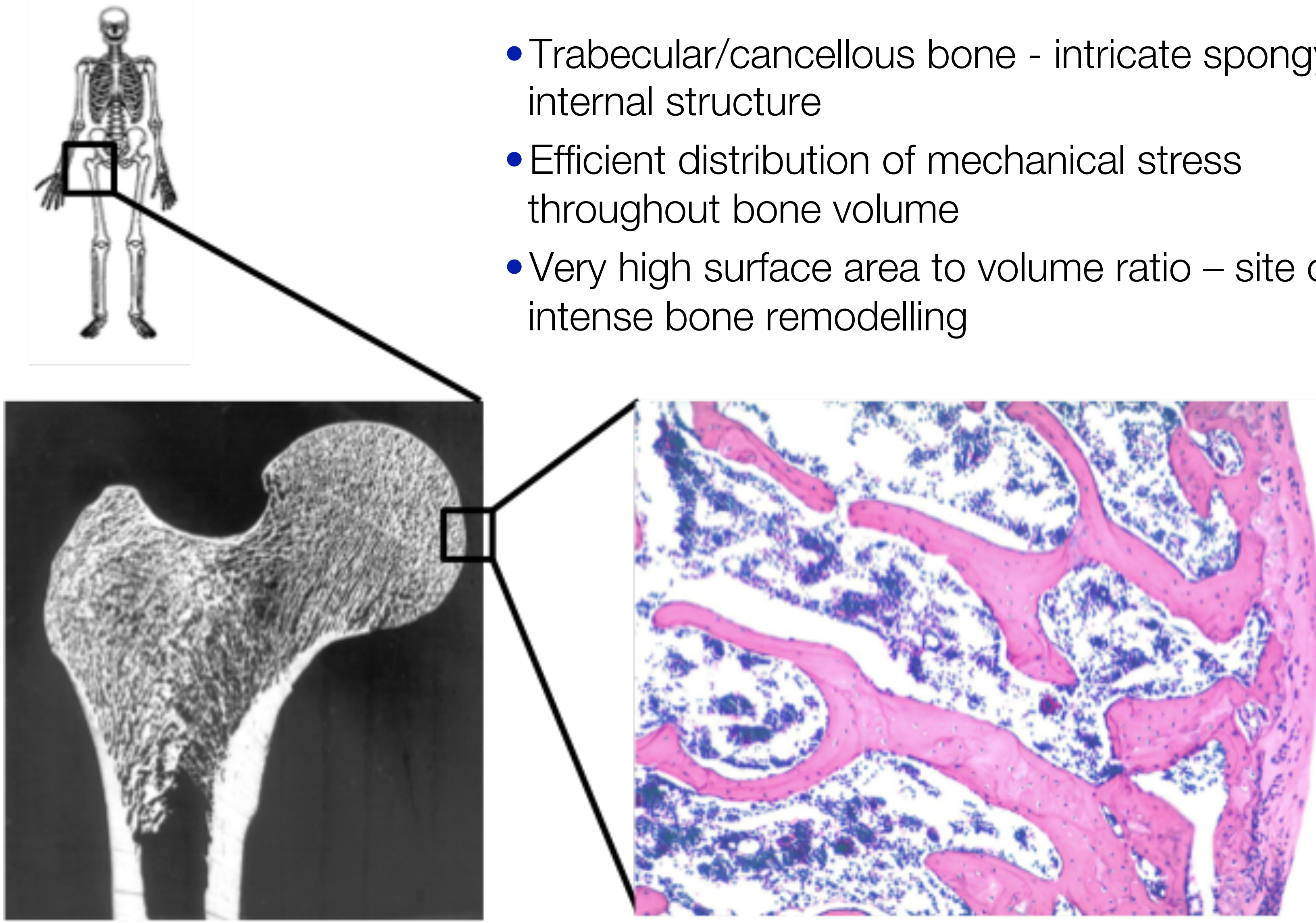

X-rays produced on Astra Gemini are ideal for imaging these bone samples

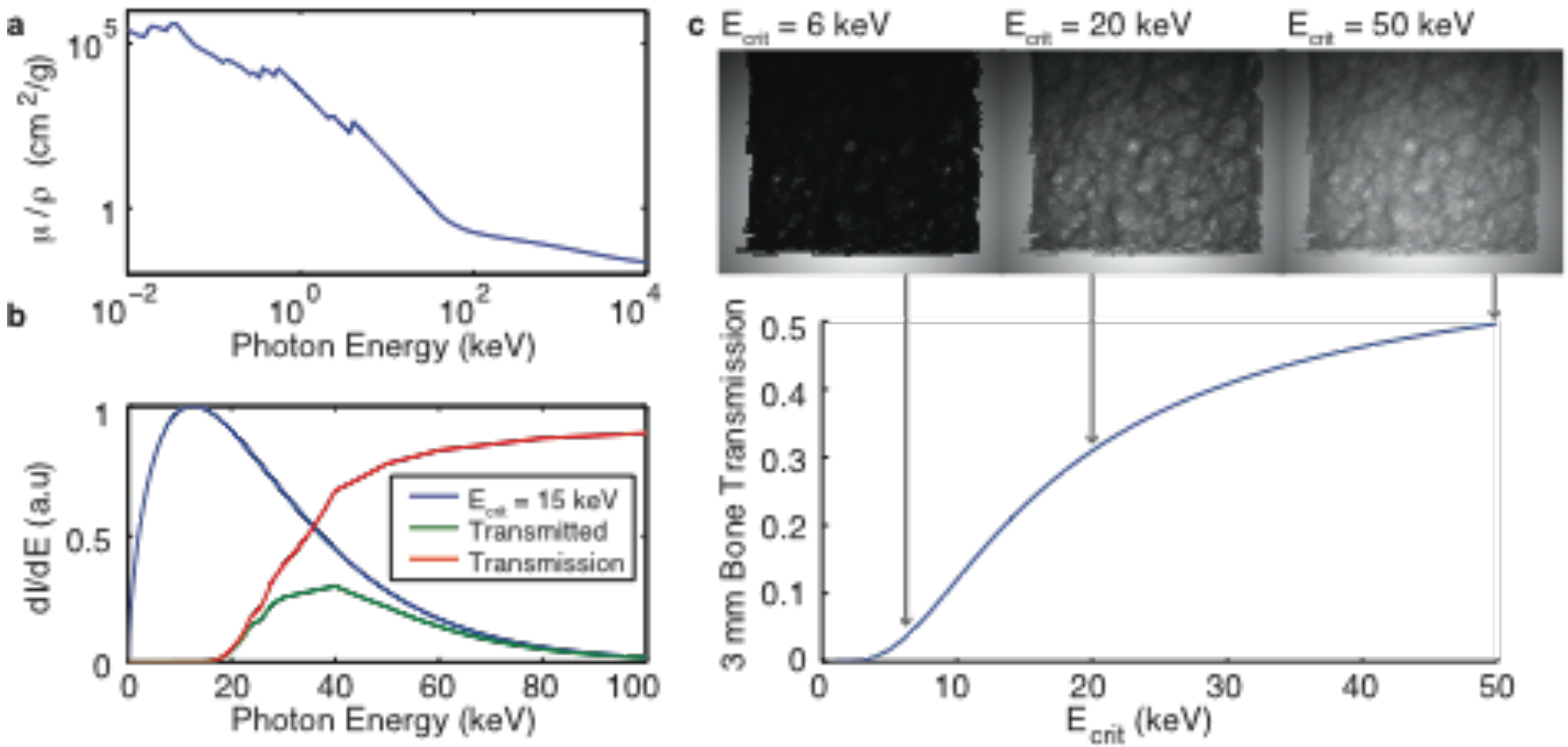

by courtesy of S.P.D. Mangles

Tomographic 3D reconstruction of human trabecular bone

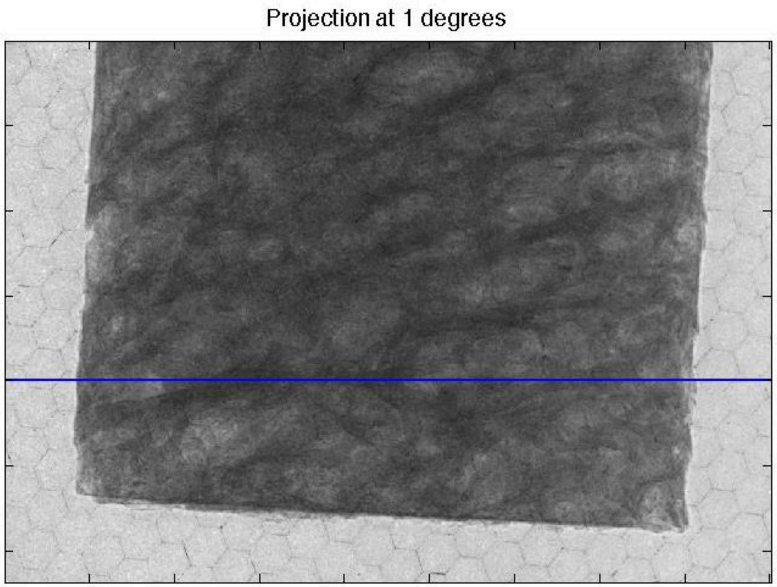

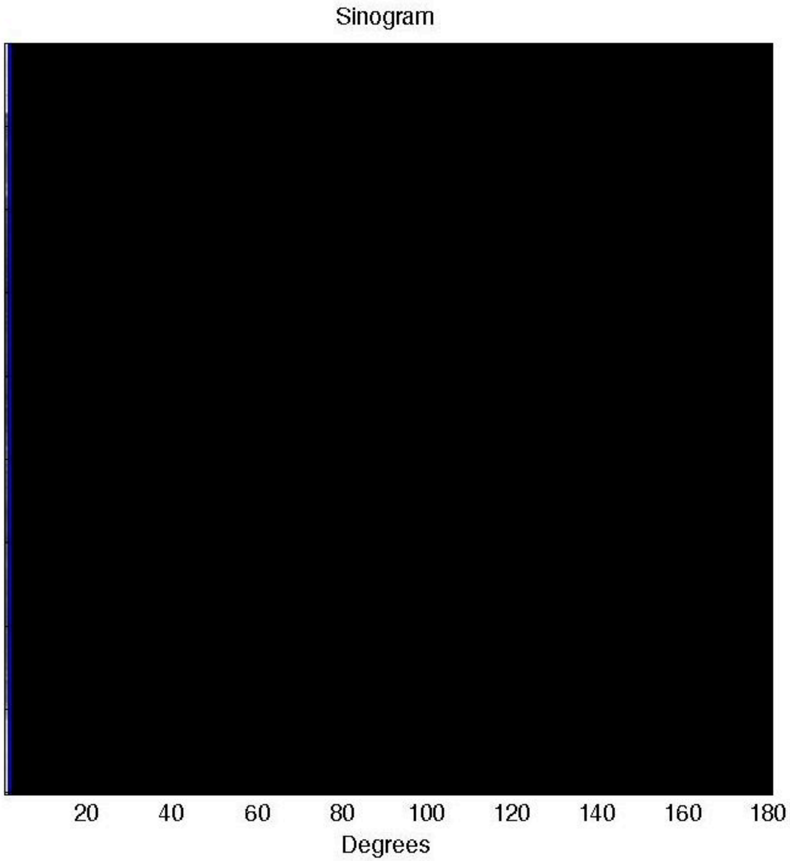

by courtesy of S.P.D. Mangles

Tomographic 3D reconstruction of human trabecular bone

analysis by Jason Cole

- Voxel size: 4.8×4.8×4.8 μm
  - –Limited by geometric magnification
  - –Resolution ≃ 50 μm
- Total scan time 4 hours
  - –@ 10 Hz laser operation this image could be achieved in 3.6 seconds
- Total dose ≃ 40 mGy
  - –potential for in-vivo studies
- Data quality already suitable for studies of osteoporosis

Thomson scattering radiation

K. Khrennikov, J. Wenz + L. Veisz group et al.

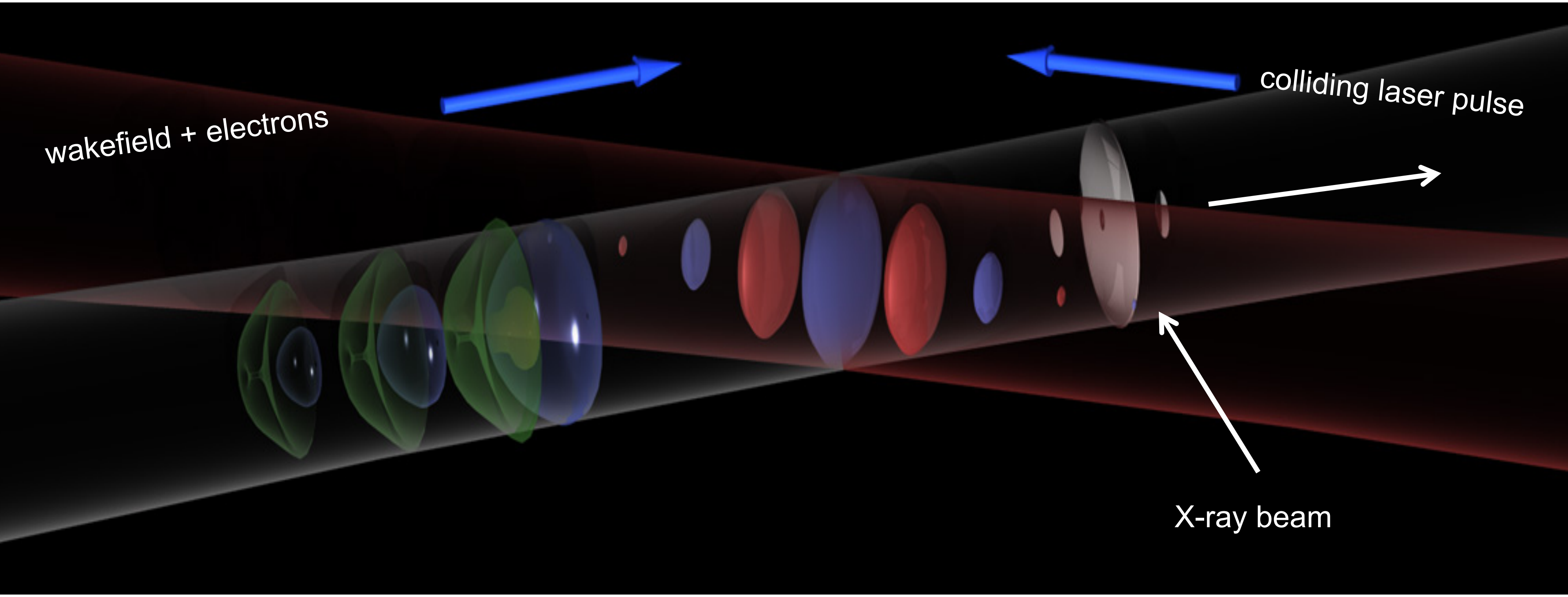

Experimental setup

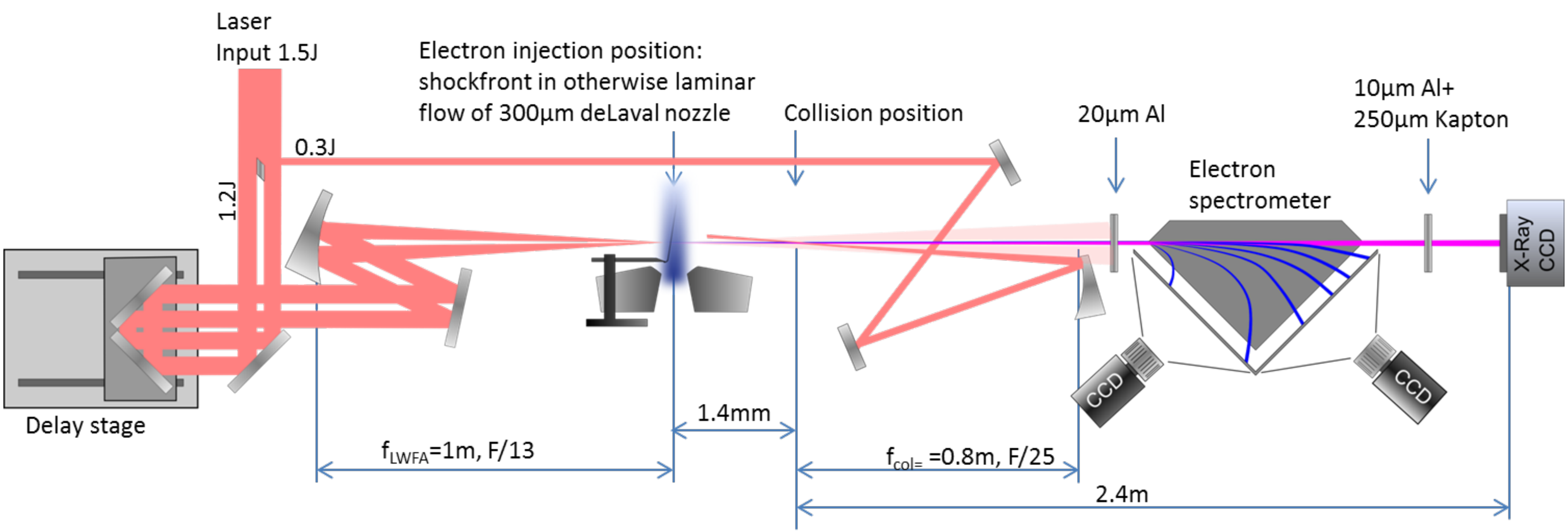

driver: 1.2 J, 28 fs, 4.2×10^{19} W/cm^2 (a_0=4.4)
colliding pulse: 0.3 J, 28 fs, 1.8×10^{18} W/cm^2 (a_0=0.9)

Electron beam size at interaction point decreases from 30 µm at 15 MeV to 17 µm at 45 MeV

Hard X-Rays recorded with an intensified camera

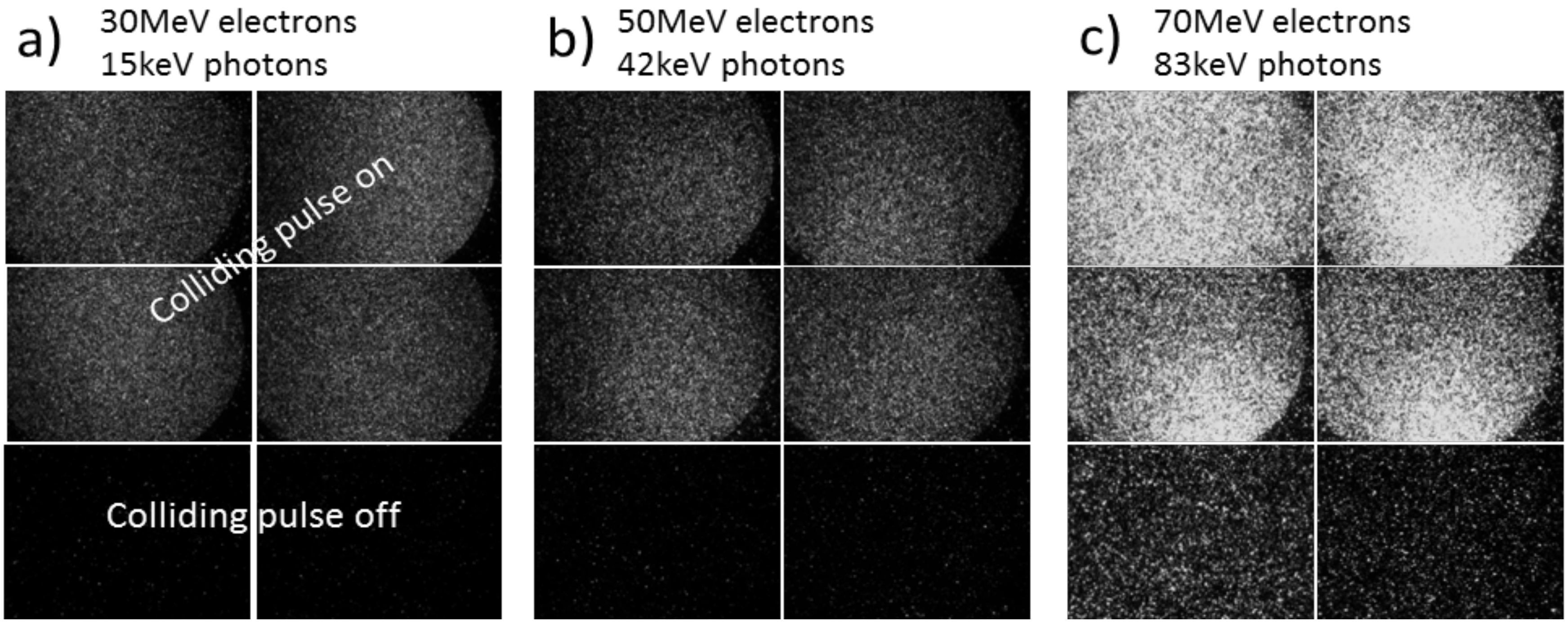

Thomson scattering (a_0=0.9)

Shock-front injected e-beams:
Electron energy (red – averaged)

X-ray energy
(red – averaged; white – expected (SPECTRA 9.0))

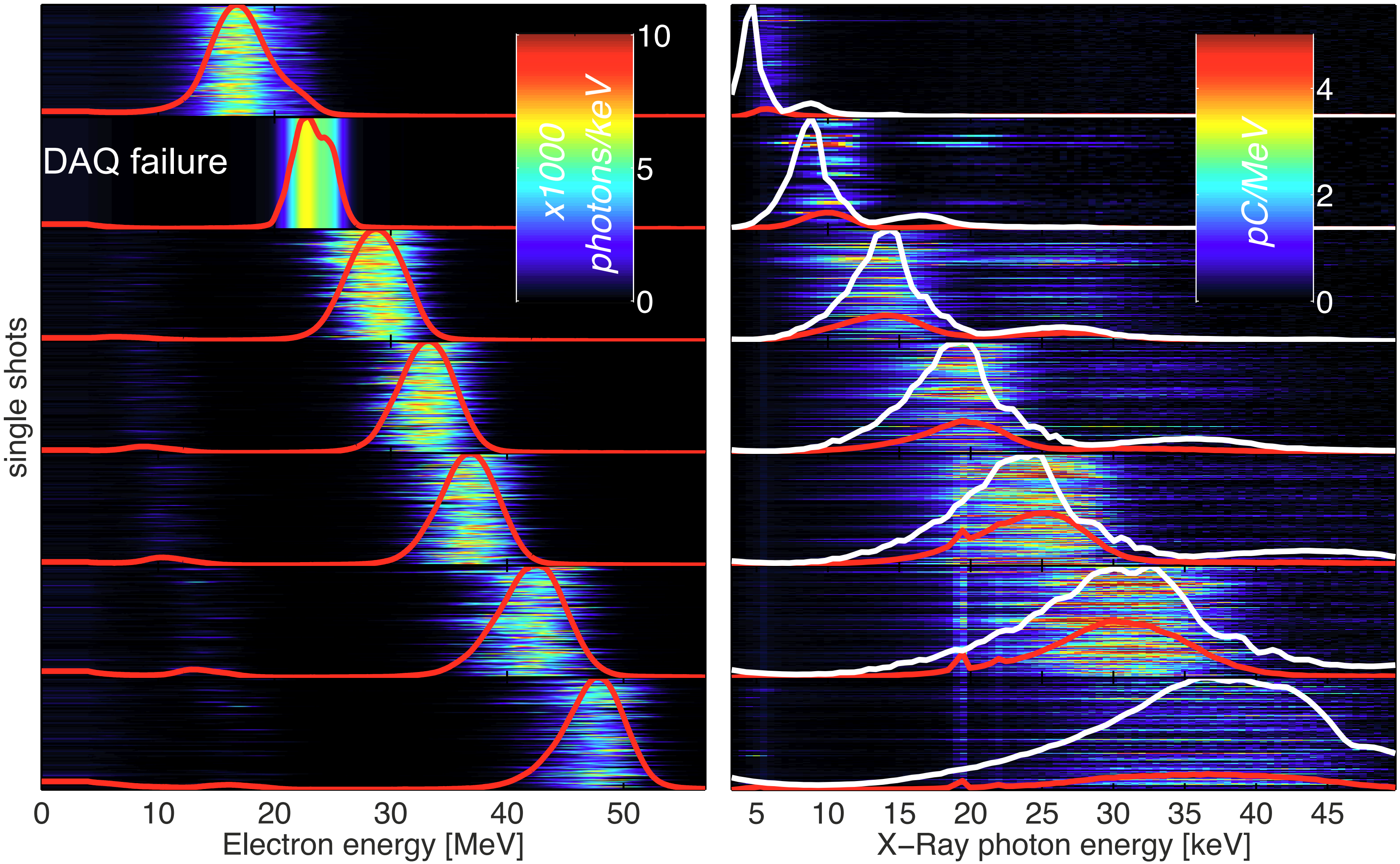

X-ray energy matches expectations from electron energy

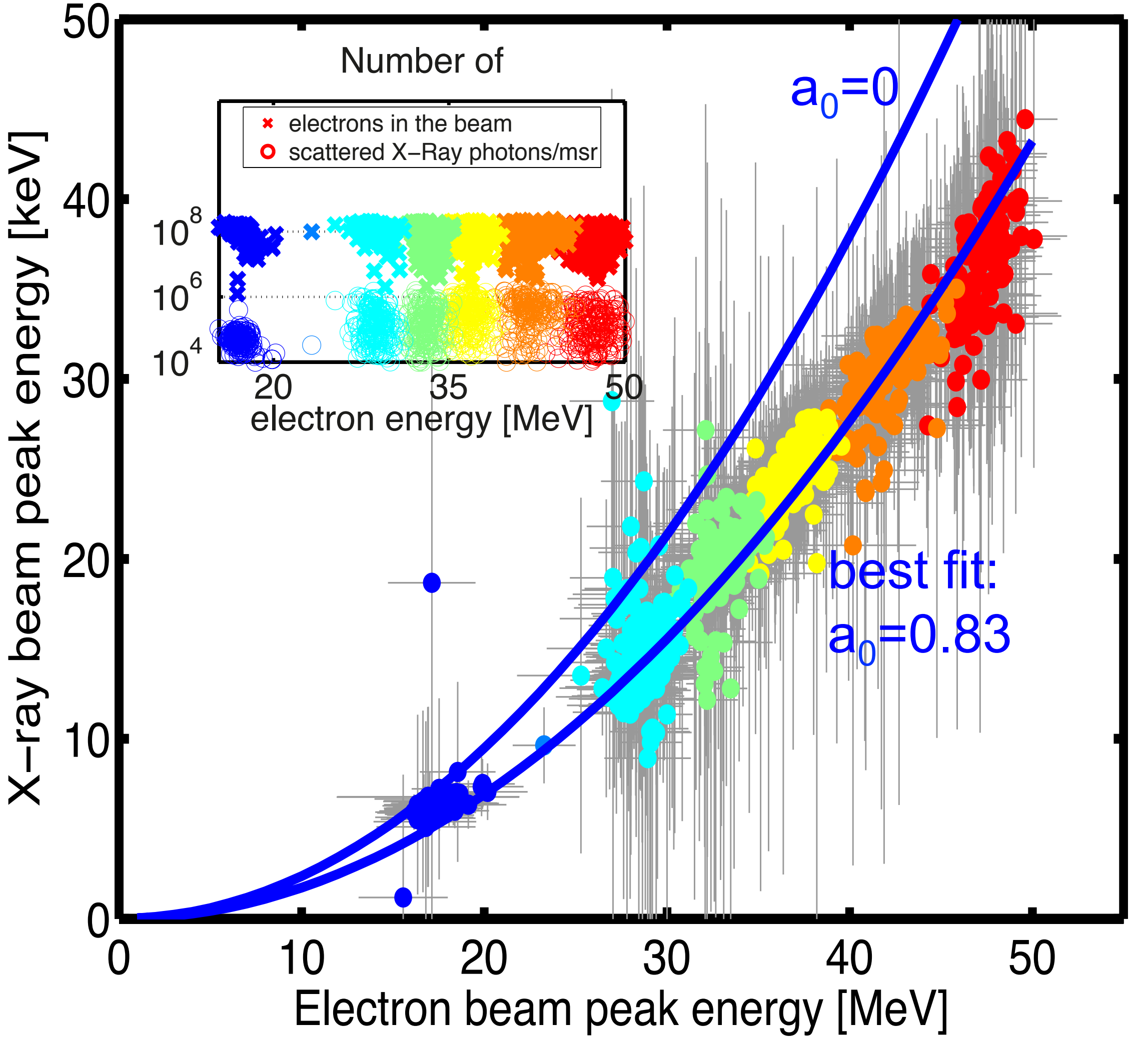

nominal a_0=0.9
(for perfect collision)

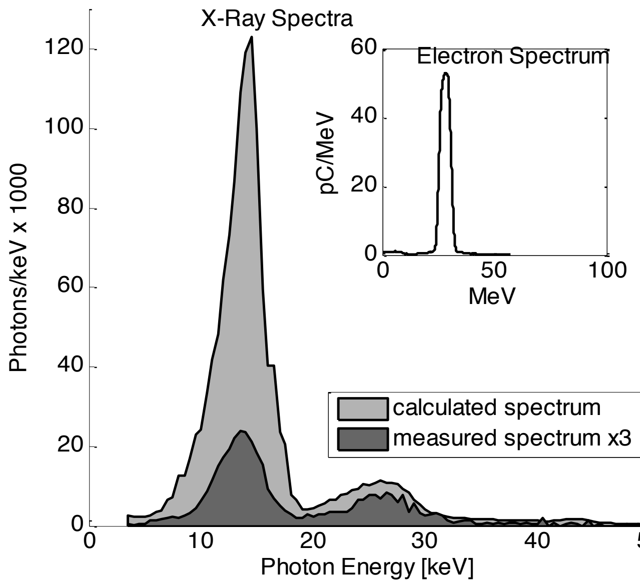

$$\lambda_{x-ray} = \frac{\lambda_l}{4\gamma^2}\left(1 + \frac{a_0^2}{2} + \gamma^2\theta^2\right)$$

Undulating with plasma fields

by courtesy of V.Malka

Laser-induced charge separation in nano-elements

Laser absorption similar to Brunel heating

Resulting e-static field: $E \simeq E_{las}(R_{wire}/r)^{1/2}$

Periodically arranged wires:

- => imposed period λ_u
- => transverse spacings control strength

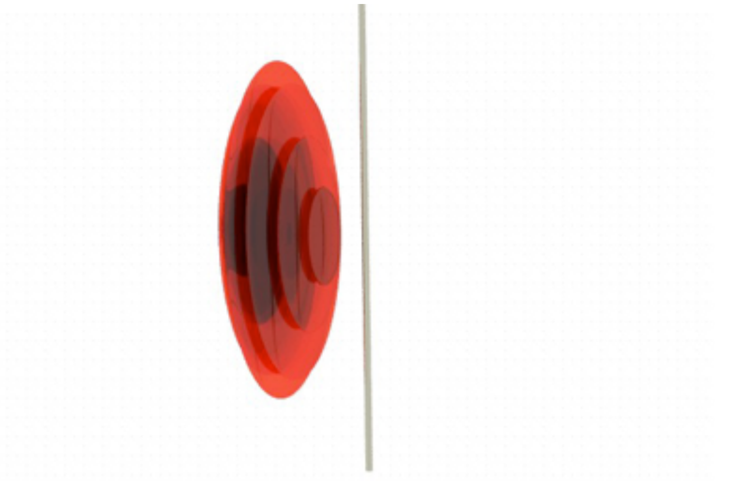

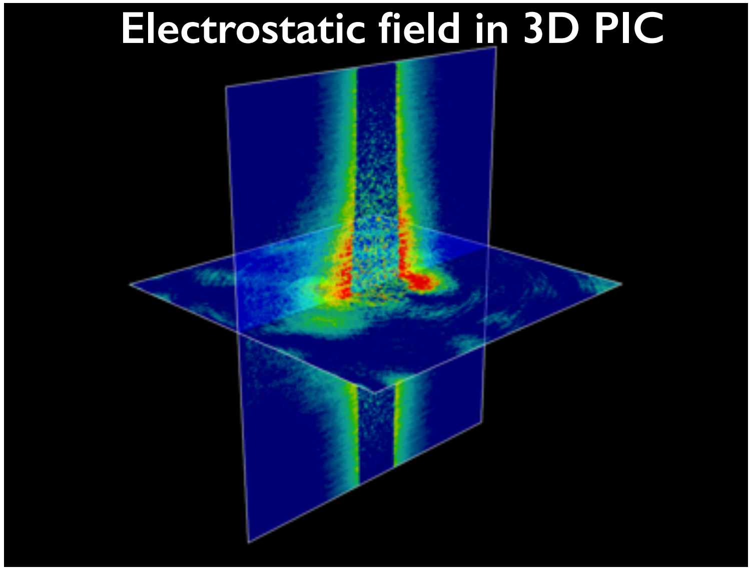

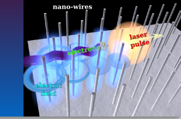

Undulating with plasma fields

by courtesy of V.Malka

2D/3D/CIRC PIC

Laser system

Pulse duration	30 fs
Pulse energy	0.7 J

Wires configuration

Diameter	0.4 μm
Period	24 μm
Transverse spacings	11μm

LPA electron beam

Emittance	0.2 mm.mrad
Energy	200-600 MeV
Energy spread	1 %

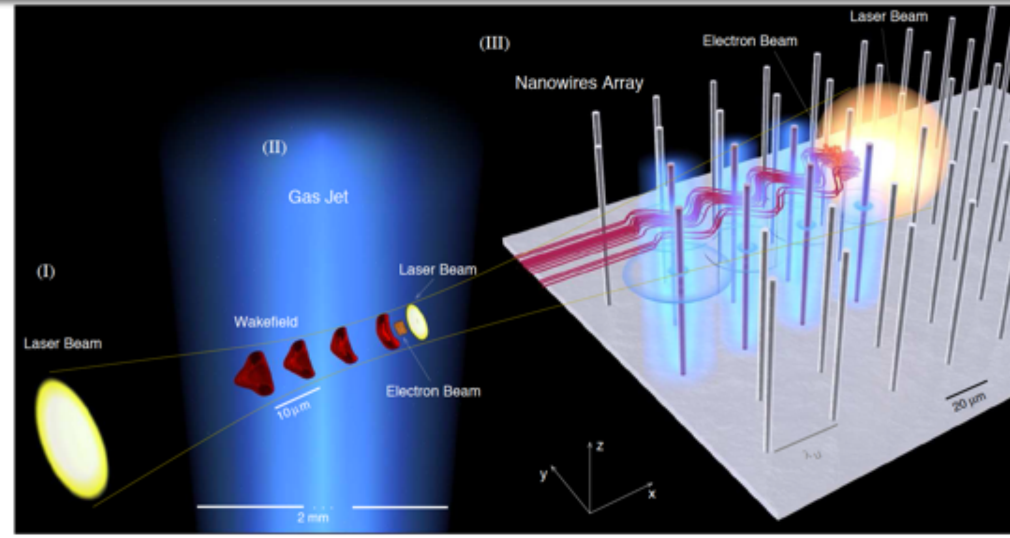

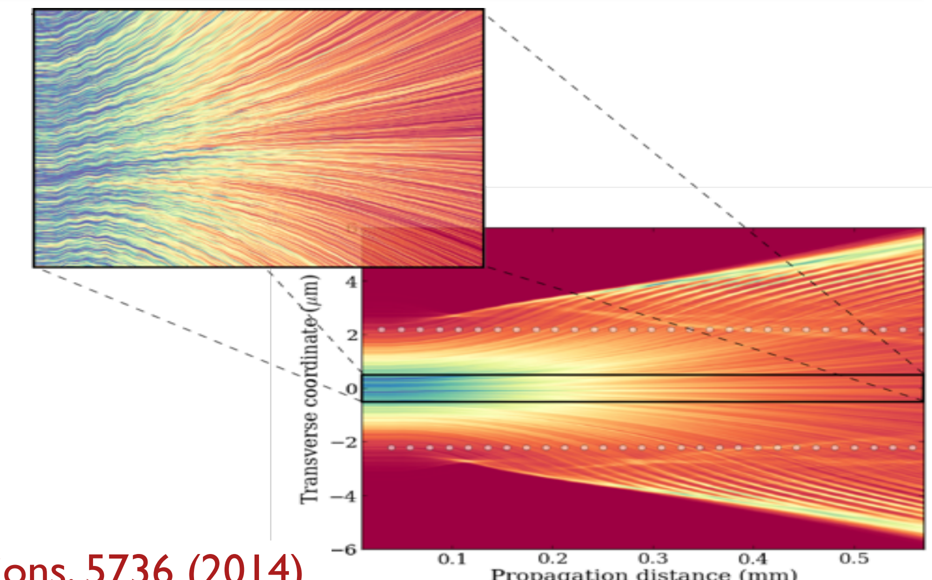

I.Andriyash *et al.*, Nat. Communications, 5736 (2014)

Undulating with plasma fields

by courtesy of V.Malka

Varying electron energy

Energy 200 / 400 / 600 MeV

Undulator emission

Photon energy 12 / 47 / 106 keV

Brightness 0.5 / 2 / 4.5×10^{23}s.u.

Angular sizes 0.85×1.7 mrad

Laser plasma nanostructured SR source

- Quasi-monoenergetic collimated spectrum
- Tunability λ_u, ε_e
- Brightness ~ γ_b^2
- Source brightness level 10^{23} s.u.
- Interaction length ≲ 1 mm

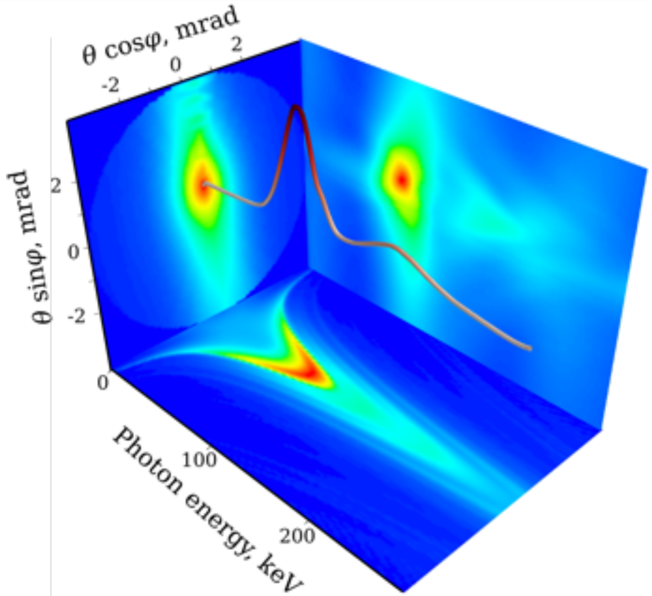

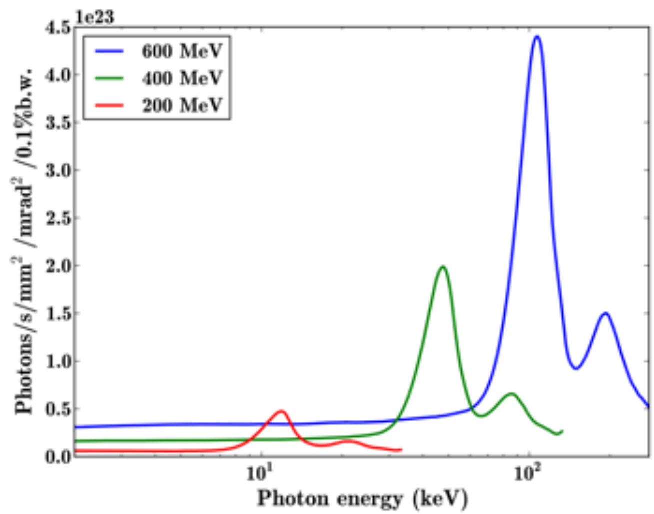

erc

loa

Japanese-French Symposium on Advanced Compact Free-Electron Lasers November 4-5 (2014),
Bureau français de la Maison franco-japonaise, Tokyo

Particle therapy with laser accelerated protons

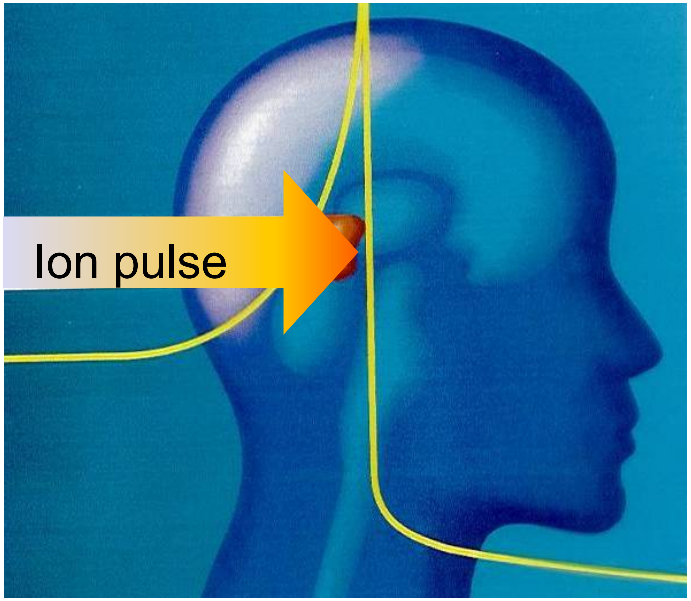

- *Favorable energy loss relation (Bragg-peak) for heavy particles*
- *Precise tools ask for precise handling and online monitoring*
- *Average power well matched and no need for low energy spread (match bandwidth to tumor profile, e.g. with pulsed magnet gantry)*

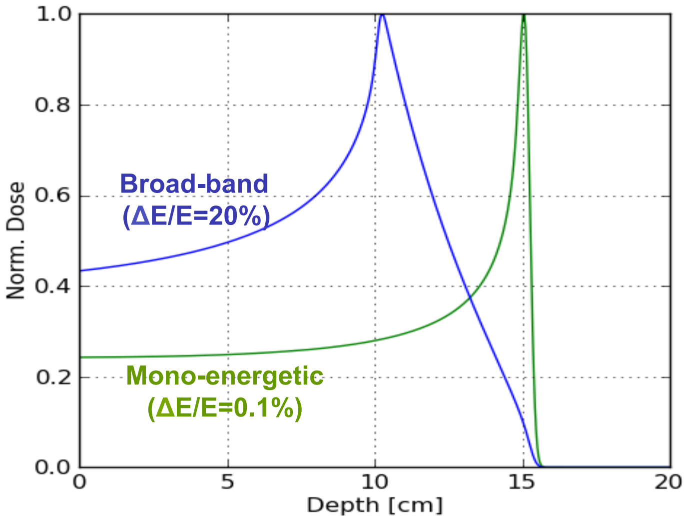

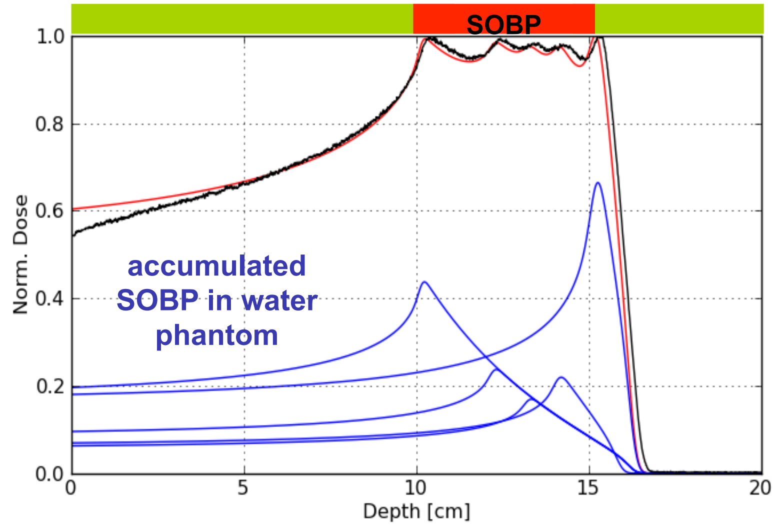

by courtesy of U.Schramm

U. Masood et al., Appl. Phys. B 117, 41 (2014)

First step: Dose controlled radiobiology

by courtesy of U.Schramm

4.1 Gy

2.7 Gy

1.5 Gy

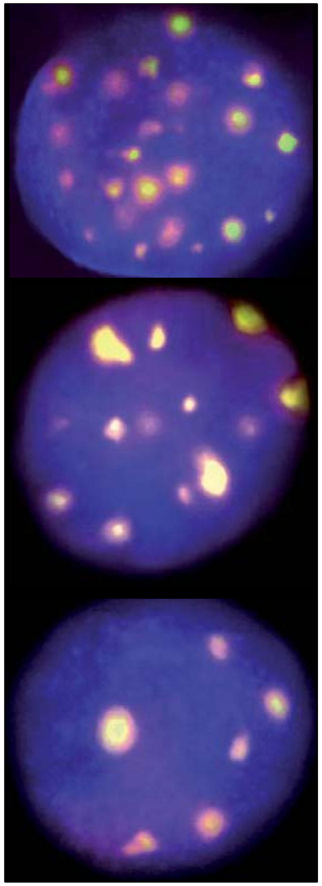

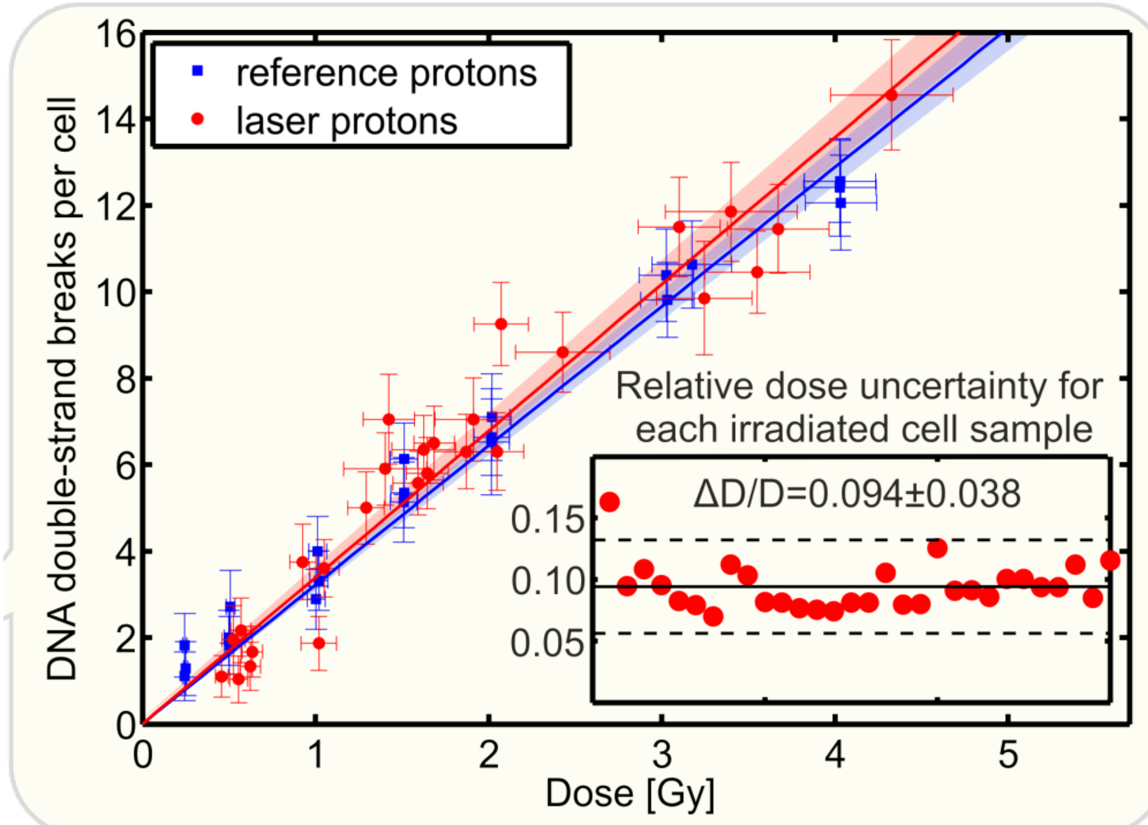

No significant difference between pulsed and continuous proton radiation (measured for sensitive head/neck SKX cell line repair activity after 24h)

Dose stability and online control for each point below 10%

Kraft et al. NJP 12 (2010) 085003, Zeil et al. Appl. Phys. B 110, 437 (2013)

oncooptics

A laser-driven nanosecond proton source for radiobiological studies

by courtesy of J. Schreiber

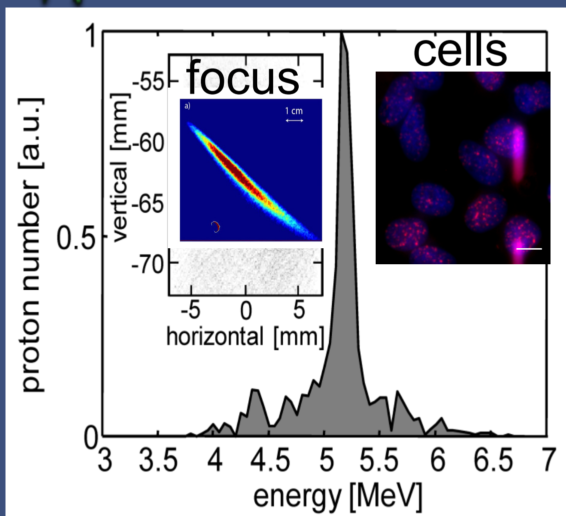

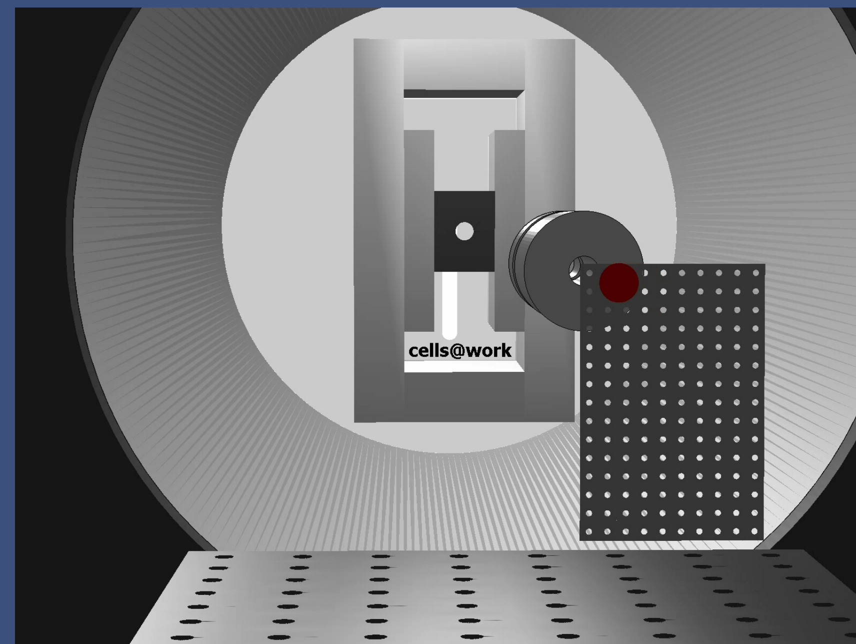

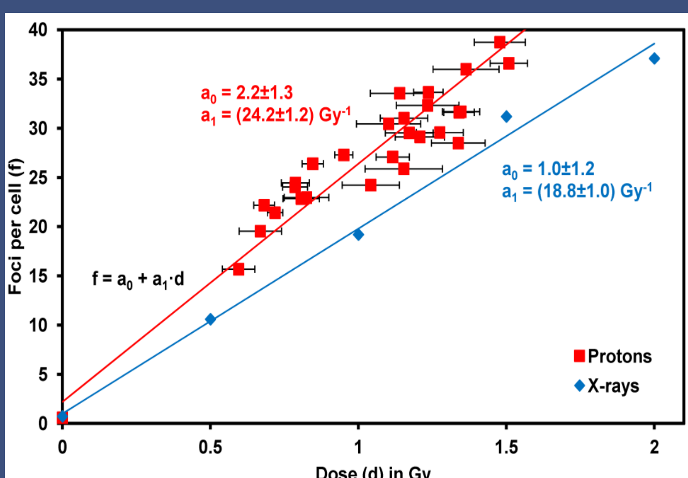

- radiate **2-7 Gy** ("lethal") dose in **one** single ns pulse
- dose response curve from a single shot
- low laser energy (400 mJ, in principle 10 Hz)
- low background radiation
    - thick foils: few microSv / shot
    - DLC: 1-2 microSv / 50 shot

Low divergence from nm DLC foils

by courtesy of J. Schreiber

ATLAS @ MPQ, 0.5 J, 30 fs

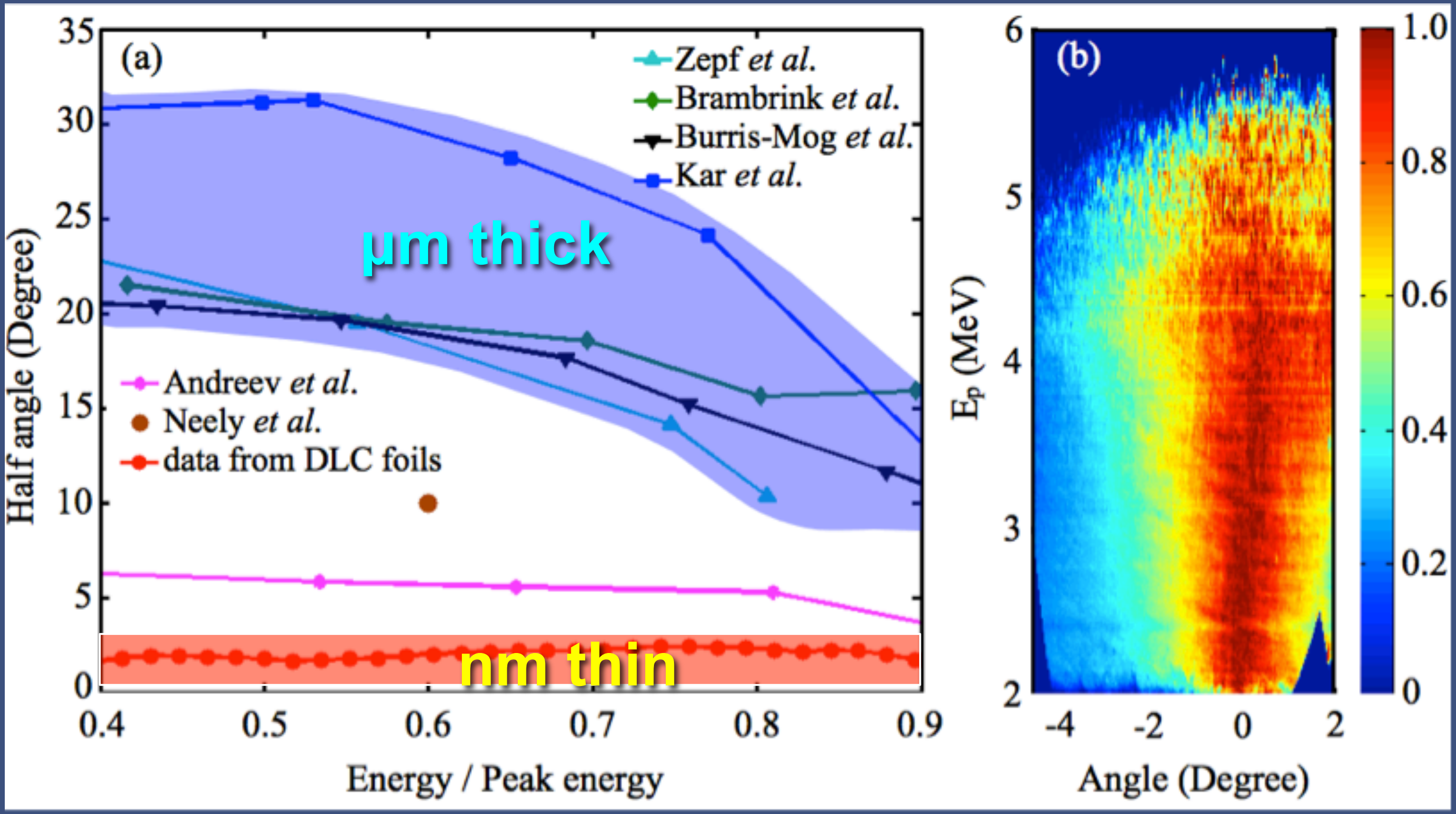

J. Bin et al., On the small divergence of laser-driven ion beams from nanometer thick foils, Physics of Plasmas 20, 073113 (2013)

Next steps: animal irradiation and scaling

by courtesy of U.Schramm

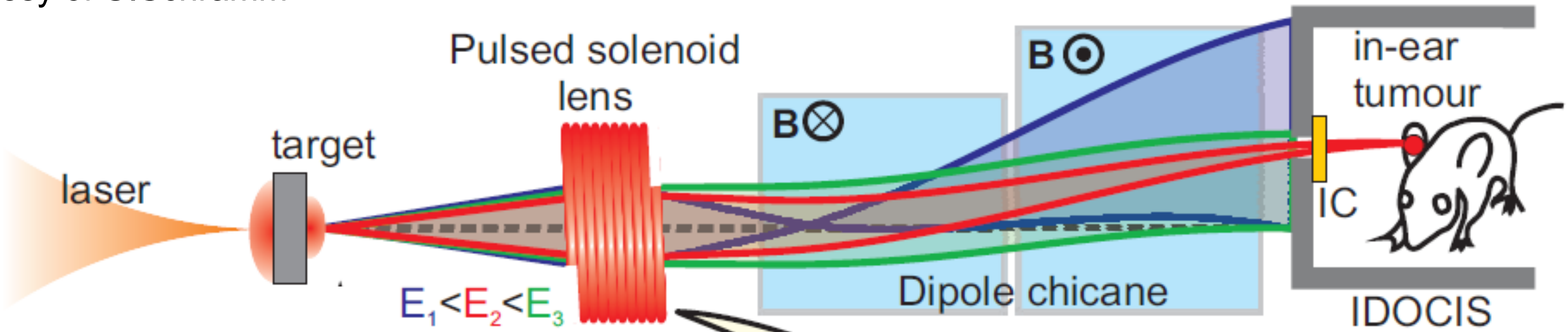

- Pulsed solenoid (energy selection and focusing demonstrated)
- Proton scaling at PW laser level

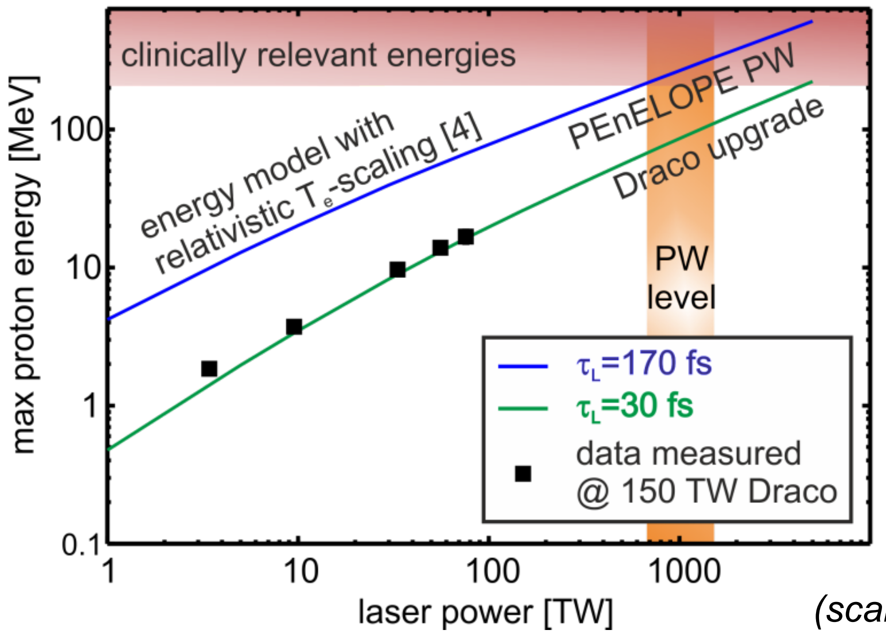

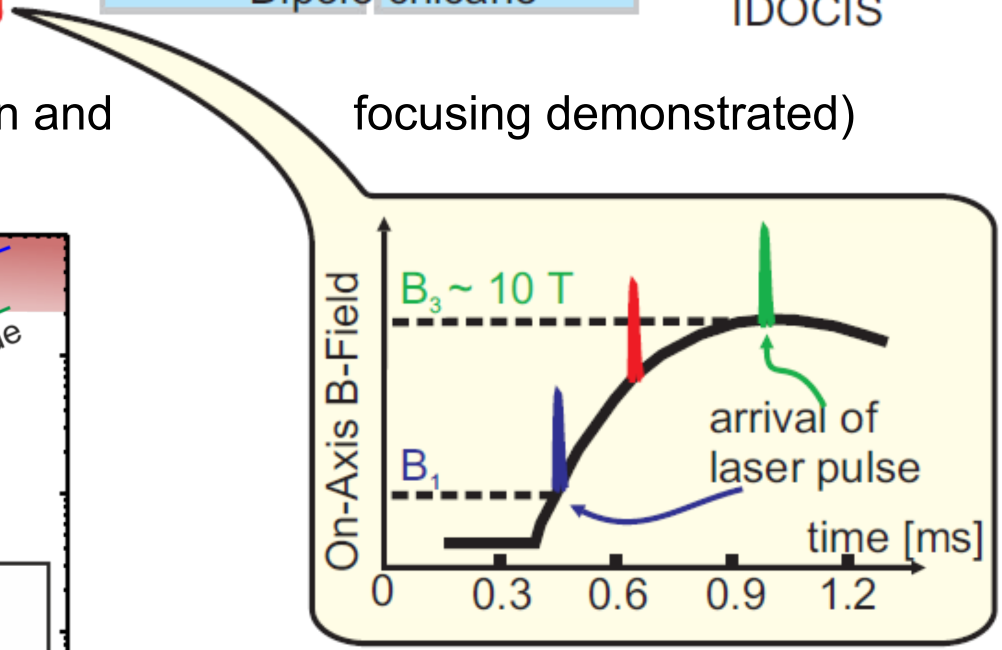

(scaling T. Kluge et al., PRL 107, 205003 (2011))

Setup for mouse ear irradiation

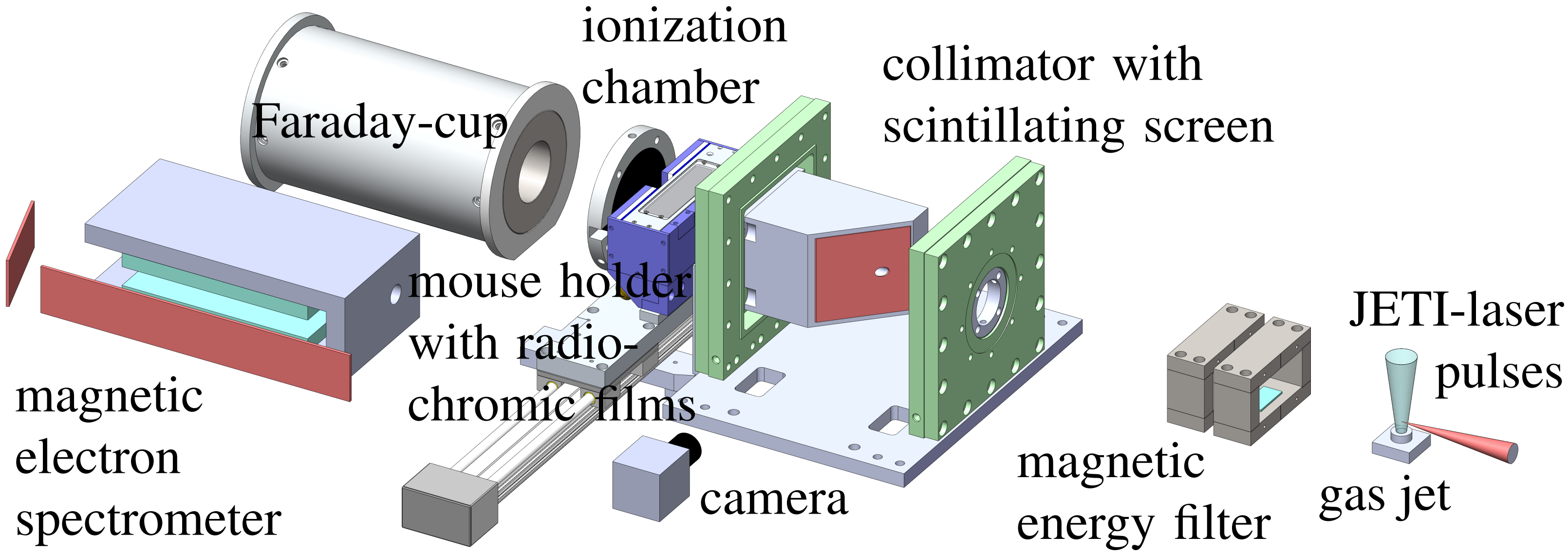

focusing	F/13
beam diameter	13 µm
intensity	8×10^{18} W/cm^2

gas jet length	2.4 mm
electron density	$1 \ldots 2 \times 10^{19}$ cm^{-3}
max. rep. rate	1 Hz

Setup for mouse ear irradiation

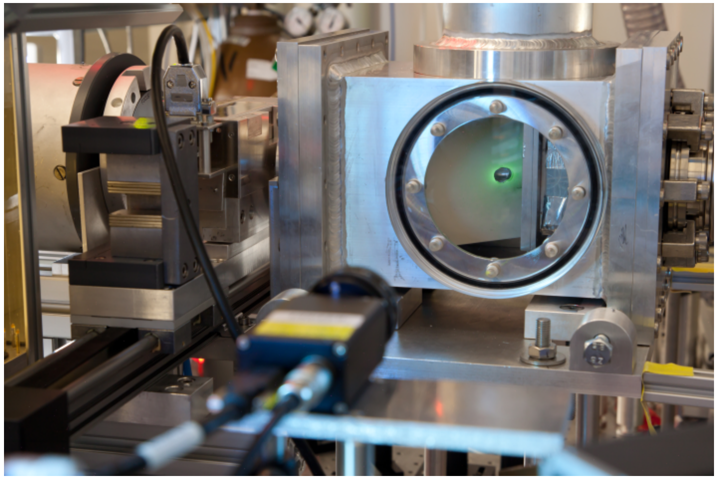

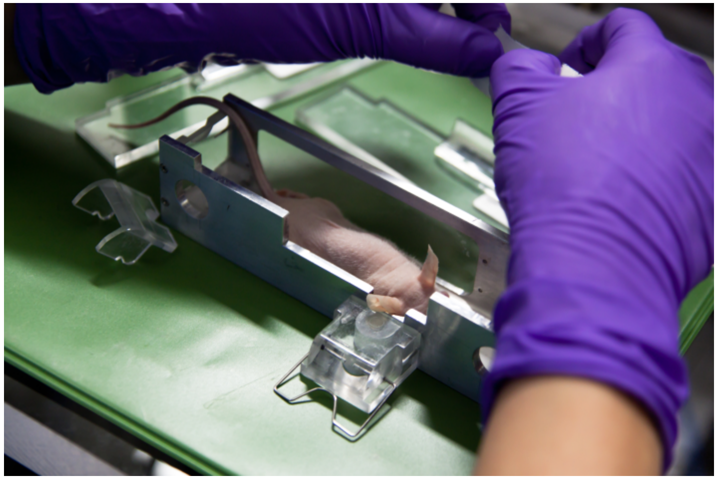

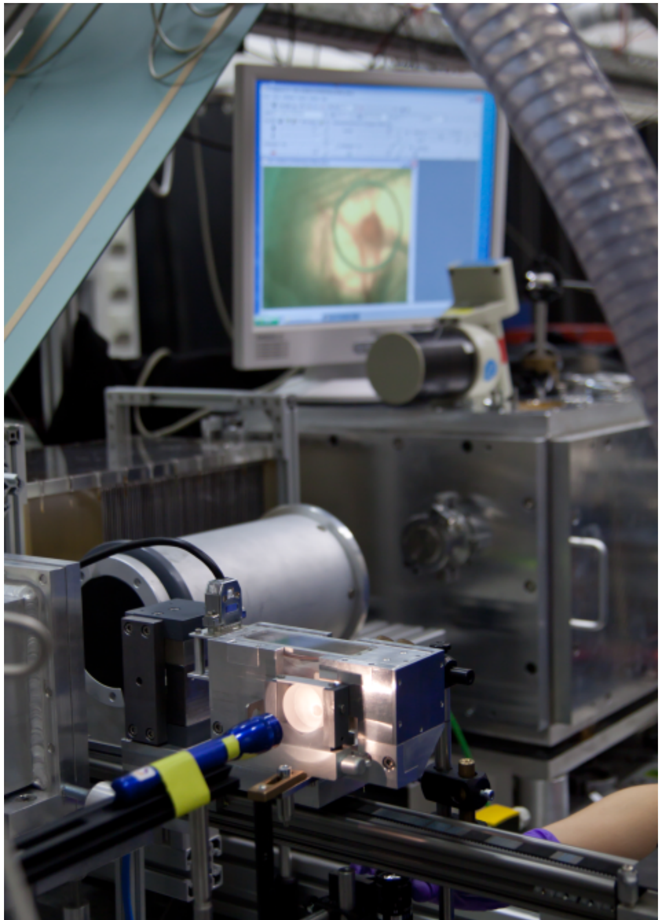

courtesy of Jens Polz, Uni Jena

	Peak brilliance (assuming 5fs duration) [photons/(s mm^2 $mrad^2$ 0.1 % bandwidth)]
Undulator	1.3×10^{17}
Betatron	2×10^{22}
Thomson	$0.02 \ldots 1.5 \times 10^{19}$ (from 5 KeV to 40 keV)

Average brilliance scales with duty cycle ($5\text{x}10^{-15}$) times the repetition rate...

⇒ rep-rated laser development!